Active Flow Control Methods for the Reduction of Trailing Edge Noise

Máté Szőke* and Mahdi Azarpeyvand†
University of Bristol, Bristol, BS8 1TR, United Kingdom

The possibility of trailing edge noise reduction using active flow control is addressed in this paper. The boundary layer is altered with the help of uniform perpendicular and inclined flow injection and suction on a long flat plate upstream of a sharp trailing edge. The flow quantities have been measured using particle image velocimetry, hot-wire anemometry, and the surface pressure fluctuations using flush mounted miniature pressure transducers. It was shown that the proposed flow control methods are capable of reducing the noise over a wide range of frequencies. It was also revealed that the perpendicular blowing is effective in shifting the energy containing turbulent structures away from the wall, resulting in a significant reduction in the surface pressure spectra. The inclined blowing control method was capable of further reducing the surface pressure spectra, while maintaining low input power requirement. The perpendicular suction control was shown to be effective in the reduction of pressure fluctuations in the mid frequency regions, which quickly penetrates to the lower frequency downstream. The inclined suction control has also lead to significant reductions in the surface pressure fluctuations over a wide range of frequencies, while the required suction rate was kept considerably low. It has also been shown that the proposed active flow control methods can reduce the spanwise correlation length of the turbulent structures near the trailing edge. In general, results have shown that all proposed active flow control techniques can effectively alter the boundary layer structure and reduce trailing edge noise.

Nomenclature

L	Streamwise length of flat plate [m]
f	Frequency [Hz]
L	Width [m]
Re	Reynolds number [−]
S_{pp}	Far-field pressure power spectrum [dB]
t	Time [sec]
u_c	Convection velocity [m/s]
u_{AFC}	Flow control velocity [m/s]
u_∞	Free-stream velocity [m/s]
$\overline{u}$	Mean velocity [m/s]
u_{rms}	Root mean square of velocity [m/s]
x	Streamwise coordinate [m]
y	Wall normal coordinate [m]
z	Spanwise coordinate [m]
γ^2	Magnitude squared coherence [-]
δ	Boundary layer thickness [m]
δ^*	Boundary layer displacement thickness [m]
θ	Boundary layer momentum thickness [m]
Λ	Turbulence length scale [m]

*PhD Student, Faculty of Engineering, University of Bristol, Bristol, United Kingdom, BS8 1TR
†Senior Lecturer, Faculty of Engineering, University of Bristol, Bristol, United Kingdom, BS8 1TR

σ	Active flow control severity [−]
τ	Time shift [sec]
φ	Phase shift [°]
ϕ_{ii}	Power spectral density of variable i [dB/Hz]
0	Subscript of baseline case
$1, 2, 3$	Subscript of x, y, z directional component
i	Subscript of variable number

AFC	Active Flow Control
BL	Boundary Layer
PIV	Particle Image Velocimetry
PPI	Pores Per Inch
RMS	Root Mean Square
TE	Trailing Edge

I. Introduction

THE past few decades have seen a rapid growth in the environmental noise pollution. Noise originated from the continuously increasing air traffic, the spread of wind farms and the rising number of turbomachinery operated (or assisted) machines have all contributed to the increase of our environmental noise. One seeking for the dominant noise source of the formerly listed applications, will find the jet noise and turbulent boundary layer trailing edge (TE) noise as of dominating noise component. After reaching the limitations of the jet noise reduction, more noise reduction effort turned toward the possibility of aerofoil noise, and in particular the TE noise reduction. To address the problem effectively, the underlying physics of TE noise generation first had to be investigated.

A deeper understanding of the TE noise generation was gained in the 1970s,[1–7] when several experiments had been conducted to quantify and investigate the trailing edge noise. Noise models, such as the BPM model,[8] TNO[9] model and Amiet's model,[5] etc., have been developed after describing the problem from a mathematical and modelling point of view. Both the experiments and the models revealed that when a turbulent boundary layer (BL) is convected over a sharp trailing edge, the hydrodynamic unsteady pressure fluctuations are scattered into sound in a dipolar manner.[6]

The increase in the aerodynamics related noise has lead to stringent noise emission regulations. These limitations currently force the various applications to restrict their operating times. It is known that the future noise regulations can not be met by the use of currently available technologies. Improvements to achieve lower noise emissions are urged by aircraft and wind turbine manufacturers to meet the standards and to improve operational costs. The need for the TE noise reduction resulted in a challenging engineering problem directing the attention toward the development of different TE noise reduction methods. The currently available approaches can be categorized as *passive* methods and *active* methods. The examples of the former one include the application of TE serrations,[10–17] TE brushes,[18,19] porous material,[20–25] surface treatments,[26–29] shape optimization and morphing,[30] etc. The efficiency of the passive methods is limited to a given range of conditions and out of this range they might introduce undesired losses. The active methods intend to overcome these limitations and push the boundaries of the achievable noise reductions.

A significant advantage of the active methods is their controllability, while external power input is required for their operation. The power intake needs to be kept low enough to ensure a desired efficient operation. Attempts on the application of AFC systems for aerodynamic tailored purposes though commercial aircraft[31] test rigs have shown that there is a significant technology gap between the required power by the AFC system and the available power from the engines.[32] This gap originates by the fact that the energy requirement of AFC for aerodynamics tailored applications scales with approximately 10^{-3} of the flow total energy. The energy of turbulence induced noise by contrast scales with 10^{-6} portion of the flow total energy, therefore it is expected that AFC systems can be more efficiently applied for noise reduction purposes.

The active methods aim for the alteration of turbulence within the BL by flow injection or suction to achieve reduction in the generated TE noise. The effect of BL injection and suction, from turbulence point of view, has already been studied by various researchers including Antonia *et al.*,[33,34] Park and Choi[35] and Oyewola *et al.*,[36–38] etc. Simulations have shown that even a low amount of flow rate (up to 10 % of free stream velocity) is sufficient for altering the boundary layer structure. Uniform flow injection can

shift the near-wall vortices away from the wall[35] and further downstream of the AFC section their size and contribution to turbulence quantities increase. Uniform flow suction can bring streamwise vortices closer to the wall, while the viscous diffusion increases resulting in the break-up of the structures and in the reduction of turbulence intensities and Reynolds shear stresses. Experiments involving larger flow rates proved that total or partial relaminarisation can be achieved above a threshold value of flow suction.[34] It was also reported that below a limiting amount of flow rate, AFC has a negligible effect on the investigated BL properties.

There is a vast number of studies on the use of passive methods for aerofoil nose reduction, while there is a limited number of papers available on active methods. Injection from the TE into the wake or flow suction from the boundary layer upstream of the TE has been of main interest.[39–44] The listed studies are either limited to low Reynolds number or to only the far field noise,[39] where it was shown that AFC can be a suitable candidate for far field noise reduction by reporting several decibels of achieved noise reduction. Detailed studies on the effect of the AFC on turbulence, and therefore on the generation of TE noise are required to find an effective way to reduce the TE noise.

Our study addresses the effect of both perpendicular and inclined blowing and suction on the main quantities determining the level of of the trailing edge noise, namely surface pressure spectrum, spanwise coherence, convection velocity, etc. Experiments involving the use of particle image velocimetry (PIV), hot-wire and flush mounted microphones have been conducted on a flat plate to measure and investigate the turbulence properties of the boundary layer and the exerted surface pressure fluctuations on the plate. The measured changes and relationship between these quantities will be brought in relation to the far field noise generation with the help of Amiet's TE noise model.

II. Experimental Set-up

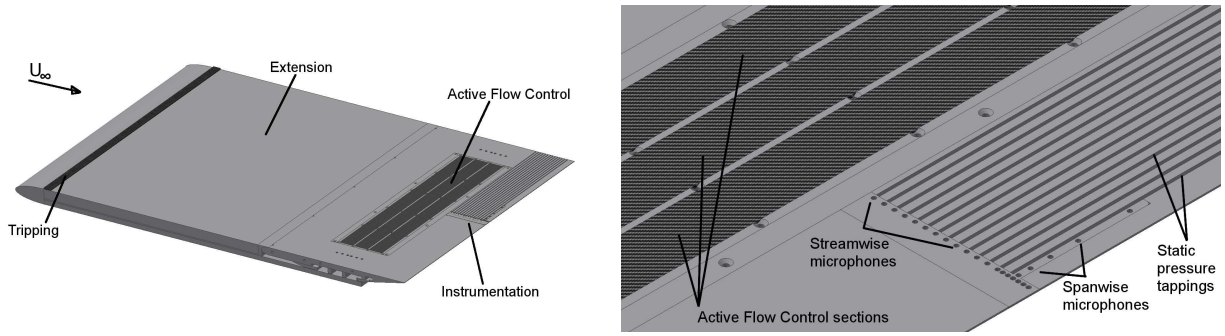

(a) Overall view of the rig

(b) Detailed view of the instrumented and active flow control area

Figure 1. Schematic view of the rig

A. Test Rig Set-up and Instrumentation

Experiments have been conducted in the open jet return-type wind tunnel facility of the University of Bristol. A long (L =1000 mm), zero pressure gradient flat plate ending in a sharp (12°) trailing edge have been built to achieve a well developed boundary layer. The overall view of the rig is depicted in Fig. 1(a). Tests have been carried out at the uniform flow velocity of $u_\infty = 10$ and 15 m/s, corresponding to a Reynolds number of 0.67 and 1.0 million based on the length of the plate. The turbulence intensity of the flow in the test section is 1 %.

Flush mounted electret microphones were used for the measurement of unsteady surface pressure fluctuations. A total number of 21 transducers were distributed both in the streamwise and spanwise directions close to the TE, see Fig. 1(b). The miniature FG-23329-P07 type Knowles microphones have been calibrated prior to the measurements, and their uncertainty was found to be ±0.5 dB within the investigated frequency range assuming normal distribution of pressure fluctuations.[45] The microphones were mounted below a pinhole with a diameter of $d = 0.4$ mm. Schewe[46] reported that keeping the dimensionless pinhole

diameter ($d^+ = du_\tau/\nu$) below $d^+ = 19$, the attenuation of the pressure signal is negligible and the discontinuity introduced on the surface does not affect the boundary layer. The current configuration resulted in d^+ values ranging between 8 and 12, therefore the pressure attenuation introduced by the pinhole is negligible. Additionally, we applied the corrections proposed by Corcos[47] during the post processing of the microphone signals. Results will be shown at four particular microphone locations along the centreline ($z = 0$) referred to as $m1$, $m2$, $m3$ and $m4$, corresponding to x/L = -0.45, -1.46, -6.5, -9.9 %, respectively (see Fig. 2).

The Dantec 55P16 type single-sensor hot-wires were used to measure the turbulence properties of the streamwise velocity component along the y axis above the microphones $m1$-$m4$. The probes were operated by a Dantec StreamWare Pro CTA91C10 module at an overheat ratio of 1.8. They were calibrated in advance of the measurements on a daily basis and their uncertainty was found to be less then 0.5 %. The data was simultaneously captured by a National Instruments PXIe-4499 system at a sampling rate of 65,536 Hz (=2^{16} Hz) for a time period of 16 seconds. The frequency resolution was set to 64 Hz during the post processing of the captured data.

Two-dimensional particle image velocimetry (PIV) was used in the low-turbulence wind tunnel facility[48] of the University of Bristol to investigate the flow structure between the AFC section and the TE of the flat plate. The Dantec DualPower 200 mJ Nd:YAG system creates a laser sheet of 1 mm thick with a corresponding wavelength of 532 nm. The time interval between the snapshots was 55 μs with a repetition rate of 2.5 Hz. The seeding of the flow was performed through the atomization of polyethylene glycol 80 resulting in particles of 1 μm diameter. A total number of 1600 images with a corresponding field view of 15 cm × 15 cm were recorded with a FlowSense 4 MP CCD camera (2078 × 2078 pixels, 14 bit) and analysed with Dantec DynamicStudio software. The applied correlation window was 16 × 16 with an overlap of 50 %.

B. Active Flow Control Methods

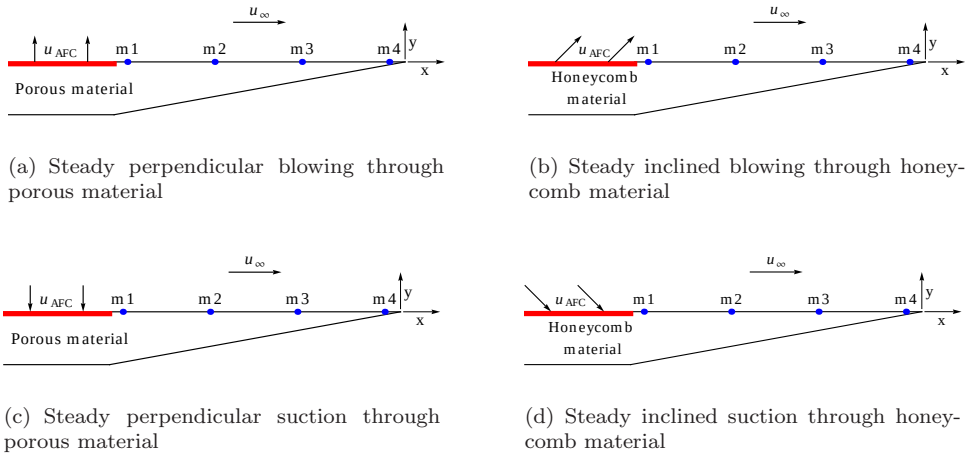

(a) Steady perpendicular blowing through porous material

(b) Steady inclined blowing through honeycomb material

(c) Steady perpendicular suction through porous material

(d) Steady inclined suction through honeycomb material

Figure 2. The schematics of the applied AFC treatments

The active flow control system has been implemented on the rig between $x/L = -12$ to -15 % upstream of the TE, corresponding to a streamwise length of $b = 30$ mm, see Fig. 1(b). In this study, we have employed four AFC methods, namely *perpendicular* and *inclined* uniform *blowing* and *suction*, see Table 1. The steady uniform perpendicular blowing and suction methods were applied through a 2 mm thick porous aluminium sheet with a porosity of 90 pores per inch (PPI). The steady uniform inclined blowing and suction was applied through a honeycomb structure built with the help of rapid prototyping technology. The width of the hexagon pores in the structure was 5 mm, the thickness of the honeycomb was 5 mm and the inclination of the pores was 30° with respect to the x-axis, see Fig. 2. The honeycomb pores were oriented upstream for the flow suction case (opposite to the flow direction) and downstream for the blowing case (in the flow direction), creating a favourable condition for the flow to enter or leave the material in both cases, see Fig. 2. In order to reduce the disturbance of the boundary layer by the surface condition of the AFC treatment, the honeycomb structure was covered by a metal wire mesh.

The severity of the suction is defined after Antonia *et al.*[34] as

$$\sigma = \frac{u_{AFC}}{u_\infty}\frac{b}{\theta_0}, \tag{1}$$

where u_{AFC} is the magnitude of the AFC velocity, u_∞ is the free-field flow velocity, $b = 30$ mm is the streamwise length of the AFC treatment and θ_0 is the momentum thickness of the non-disturbed boundary layer, i.e. σ relates the momentum of the boundary layer to the momentum of the AFC. Assuming that for turbulent boundary layers the momentum thickness can be approximated as $\delta \approx 10\,\theta$, one can infer that $\sigma = -10$ is equivalent to the elimination of the boundary layer, although Antonia *et al.*[34] reported relaminarisation at $\sigma = -6.5$.

It was revealed during the initial wind tunnel tests that the investigated active flow control methods can be effectively applied on boundary layers of different thickness. To properly study the effects of the AFC system, it is desirable to have a thick BL for the blowing case and a thin BL for the suction case. Mounting (a) an 80 grit 40 mm long sandpaper resulted in a well-developed thin boundary layer and (b) a 25 PPI 10 mm thick, 20 mm long porous aluminium block resulted in a thick boundary layer, see Table 1.

Table 1. Properties of the baseline flow and active flow control at the beginning of the flow control section

Case	Applied tripping	u_∞	θ_0	δ_0	Re_{θ_0}	Applied σ values
		[m/s]	[m]	[m]	[–]	[–]
Steady perpendicular blowing	Porous block	15	12.9	109.8	13,000	0.22, 0.62
Steady inclined blowing	Porous block	10	8.68	73.04	5,700	0.9, 1.1
Steady perpendicular suction	Sandpaper	10	1.8	20.66	1,200	-3, -9
Steady inclined suction	Sandpaper	10	2.2	25.65	1,500	-3.2, -4.2

C. Amiet's Trailing Edge Noise Model

The dominant quantities driving the TE noise generation can be readily found from the TE noise models. One of the most widely used analytical models is that of Amiet.[5] The model aims to link the surface pressure fluctuations (ϕ_{pp}) to the far-field pressure power spectra (S_{pp}). It assumes frozen turbulence and large span to chord ratio. Amiet defined the far-field pressure power spectrum as

$$S_{pp}(x, 0, z, \omega) = \left(\frac{\omega c y}{4\pi c_0 \sigma^2}\right)^2 \frac{L}{2} \left|\mathcal{L}\right|^2 \Lambda_3(\omega)\phi_{pp}(\omega, 0). \tag{2}$$

As seen in Eq. (2), the most important component in the model, driving the TE noise generation, is the surface pressure fluctuations (ϕ_{pp}) exerted on the surface by the turbulent boundary layer. These fluctuations, according to the model, are driven by the boundary layer and its turbulence properties, such as turbulent length scales (Λ_2 and Λ_3), turbulent shear stresses ($\partial u/\partial y$) and convection velocity (u_c). We aim to measure a number of these quantities and evaluate the effect of the proposed AFC methods on these parameters. Additional turbulence measures such as Reynolds shear stresses, frequency-energy content of the boundary layer, temporal cross and auto-correlation can also indicate the changes in the generated TE noise. A number of these quantities will be presented and discussed in the following sections.

III. Results

In this section the measured flow and surface pressure data will be presented and discussed. The hot-wire probes were positioned above the $m1$-$m4$ locations and they were traversed within the boundary layer whilst data were collected simultaneously from the microphones and the hot-wire. The schematic of the trailing edge with the microphones is presented in Fig. 2. The effects of the proposed AFC techniques will be discussed and the physical causes of any significant changes observed will be analysed. In what follows, we shall first present the results of the steady blowing, followed by the steady suction results.

A. Steady Uniform Perpendicular Blowing

Table 2. Boundary layer properties for the perpendicular blowing cases at location $m1$

BL blowing	u_∞	δ	δ^*	θ	u_τ	Re_θ
$m1$	[m/s]	[mm]	[mm]	[mm]	[m/s]	[−]
$\sigma = 0$	15	109.75	16.54	12.89	0.555	13,000
$\sigma = 0.22$		111.22	22.08	10.98	0.540	11,100
$\sigma = 0.62$		107.04	24.07	10.91	0.525	11,000

The effects of blowing on the boundary layer structure can be identified by studying the mean streamwise ($\overline{u}/u_\infty$) and root mean squared (u_{rms}/u_∞) velocities. These quantities are studied using both the hot-wire and PIV results, as shown in Figs. 3 to 5. The wind tunnels used for the PIV tests and hot-wire measurements were different, causing some slight discrepancies in the scaling of the results, but it does not have a significant effect on the flow quality.

The PIV results presented in Fig. 3 give a good understanding on the flow structure before and after flow injection. The results indicate that the perpendicular blowing results in a flow separation downstream of the AFC section and that the flow reattaches before reaching the TE for both of the investigated blowing rates. The size of the recirculation zone is proportional to the introduced amount of fluid. The images reveal that the streamlines are only slightly affected by the blowing above the separation zone. We can therefore expect that the boundary layer thickness is not significantly increased by blowing. Results have also shown that the turbulence intensity (U_{rms}/u_∞) first decreases compared to the baseline case downstream of the AFC section, but further downstream, after the recirculation eye, there is a significant increase in U_{rms} due to the presence of shear layer above the separation zone. The same observations were made by Park and Choi[35] with respect to the flow turbulence content for the application of blowing.

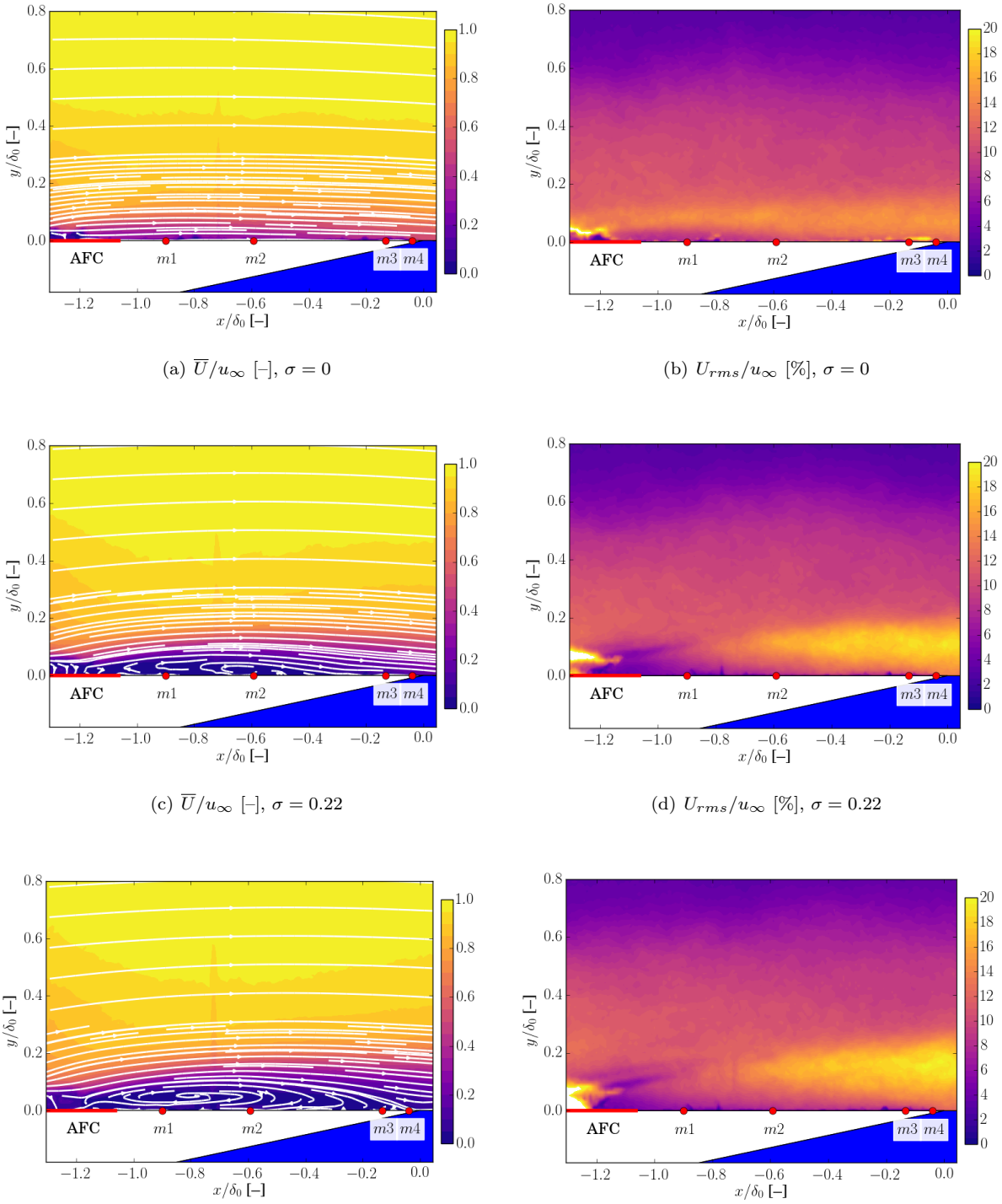

(a) $\overline{U}/u_\infty$ [–], $\sigma = 0$

(b) U_{rms}/u_∞ [%], $\sigma = 0$

(c) $\overline{U}/u_\infty$ [–], $\sigma = 0.22$

(d) U_{rms}/u_∞ [%], $\sigma = 0.22$

(e) $\overline{U}/u_\infty$ [–], $\sigma = 0.62$

(f) U_{rms}/u_∞ [%], $\sigma = 0.62$

Figure 3. Velocity magnitude with streamlines (left column) and flow energy content in percent of free-stream velocity (right column) measured with the use of PIV downstream of the AFC section for the $\sigma = 0, 0.22$ and 0.62 blowing cases

Figure 4 presents the mean velocity profiles for two different blowing rates ($\sigma = 0.22$ and 0.62) and the baseline case measured at the $m1$-$m4$ locations. The newly introduced fluid layer within the BL resulted in a significant momentum deficit below $y/\delta_0 = 0.2$ at all locations, and a velocity overshoot at locations $m1$ and $m2$ between $y/\delta_0 = 0.2 - 0.6$. This effect on the BL profiles, similarly to what Park and Choi[35] reported, is due to the uplift of the turbulent structures. These observations will be further discussed with the help of the streamwise velocity power spectral density plots presented in Fig. 6. We can find an inflexion point in the velocity profiles of the blowing cases at location $m1$ close to the surface ($y/\delta_0 < 0.1$), indicating a separated flow, in agreement with the PIV results in Fig. 3. This inflexion was not experienced upstream of the TE indicating that the flow has reattached before reaching the TE. We can also see that as the boundary layer profiles are almost identical above $y/\delta_0 = 0.6$ for all locations, the currently applied blowing does not have a significant effect on the boundary layer thickness, as shown in Table 2. The boundary layer momentum and displacement thickness (θ, δ^*) were, however, significantly affected. This indicates that the treated BL carries a significantly less momentum than the baseline case. We can conclude from the $\overline{u}$ profiles that the introduced flow has a local near-wall effect on the boundary layer structure, whose effects are felt further downstream.

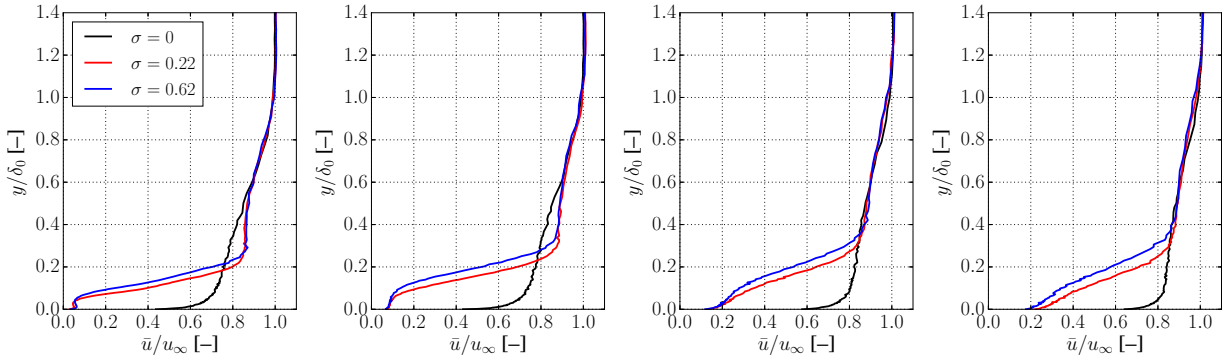

(a) $\overline{u}$ profiles at $m1$ (b) $\overline{u}$ profiles at $m2$ (c) $\overline{u}$ profiles at $m3$ (d) $\overline{u}$ profiles at $m4$

Figure 4. Mean velocity profiles downstream of the active flow control section at locations $m1 - m4$ for the blowing flow control cases

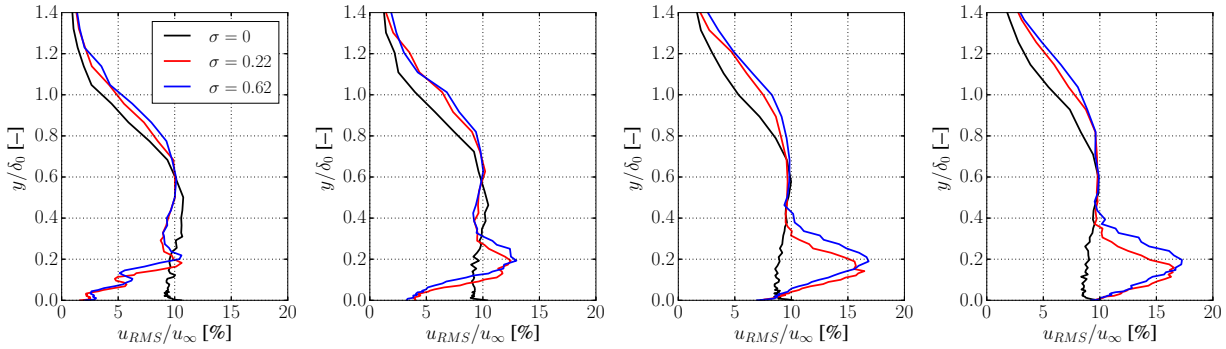

(a) u_{rms} profiles at $m1$ (b) u_{rms} profiles at $m2$ (c) u_{rms} profiles at $m3$ (d) u_{rms} profiles at $m4$

Figure 5. Root mean square velocity profiles downstream of the active flow control section at locations $m1 - m4$ for the blowing flow control cases

Figure 5 shows the energy content of the streamwise velocity component (u_{rms}) within the boundary layer at the locations $m1$-$m4$. A significant reduction in the velocity rms profiles is observed at the location $m1$ below $y/\delta_0 = 0.6$, while the flow energy content shows an increase downstream at locations $m2 - m4$ in the recirculation zone ($y/\delta_0 = 0 - 0.4$). The point $y/\delta_0 \approx 0.6$ separates two flow regions at each location: below $0.6\delta_0$, where the effect of blowing on u_{rms} stems from the newly introduced flow layer, and above $y/\delta_0 \approx 0.6$, where the increase in u_{rms} is originated from the uplifted vortices. The presence of a shear layer is clear from the shape of the four velocity rms profiles. They have a pointed shape below $y/\delta_0 \approx 0.4$ with a

is clear from the shape of the four velocity rms profiles. They have a pointed shape below $y/\delta_0 \approx 0.4$ with a peak located at $y/\delta_0 \approx 0.2$. This layout, being a clear effect of blowing, encourages the flow to develop larger, energy containing turbulent structures as we move towards the TE. Similarly, Park and Choi[35] reported a growth in the turbulence intensity downstream of the blowing section and they attributed this effect to the reduced viscous diffusion.

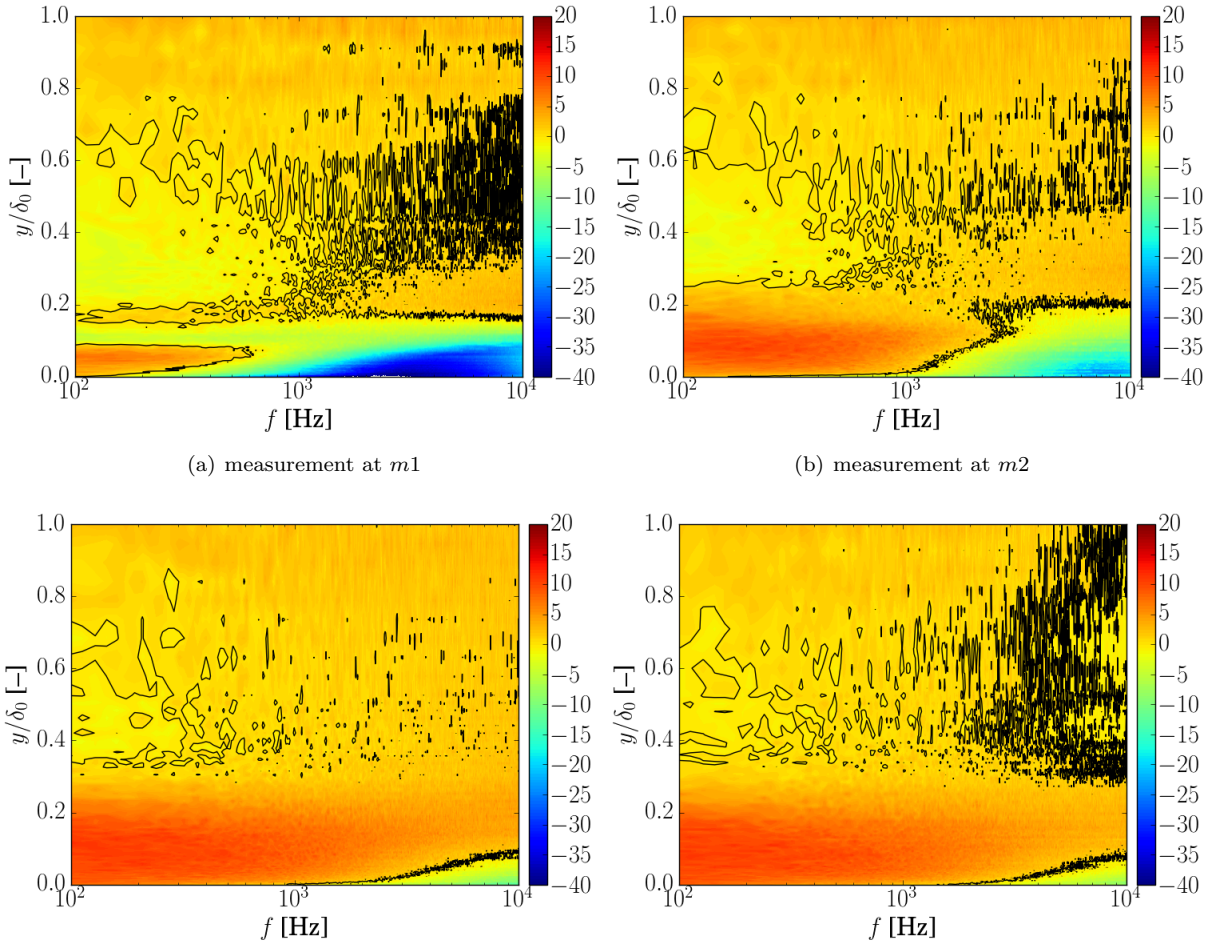

(a) measurement at $m1$

(b) measurement at $m2$

(c) measurement at $m3$

(d) measurement at $m4$

Figure 6. Change in the power spectra of the u velocity component within the boundary layer ($\Delta\phi_{uu}$ [dB/Hz]) downstream of the active flow control section at locations $m1 - m4$ for the $\sigma = 0.22$ blowing flow control case

The changes in the energy-frequency content of the u velocity component with respect to the baseline case ($\sigma = 0$) are shown in Fig. 6 for the $\sigma = 0.22$ case within the boundary layer ($\Delta\phi_{uu} = \phi_{uu,\mathrm{AFC}} - \phi_{uu,\mathrm{Baseline}}$ [dB/Hz]). The black contour lines in the plots represent the level $\Delta\phi_{uu} = 0$ dB/Hz, separating the areas of energy increase and decrease. Following the discussion on flow energy content seen in the PIV images and hot-wire results, it is visible that the injected fluid could penetrate slightly less than $0.2\delta_0$ into the BL. This is indicated by the vertical zero level contour line at $m1$ slightly below $0.2\delta_0$. The energy content of the streamwise velocity component was significantly reduced below $0.2\delta_0$ at the location $m1$ in the higher frequency region. There is a slight increase for frequencies below 600 Hz in this area, indicating that the flow at this location still has a larger energy content in the corresponding frequency range than the baseline case. From aeroacoustic point of view, it is important to reduce the energy content in the flow, therefore the goal is to introduce a flow into the BL that carries low energy content. Further reduction is observed at $m1$ and $m2$ between $y/\delta_0 = 0.2$ and 0.6. This vertical range coincides with the formerly experienced velocity overshot region of $\overline{u}$ in Figs. 4(a) and 4(b). Reduction in the formerly presented u_{rms} profiles at $m1$ and $m2$ were observed at the same $y/\delta_0 = 0.2 - 0.6$ range. As we move towards the locations $m2$-$m4$, the development of larger structures is confirmed by the energy increase in the area of $y/\delta_0 < 0.3$ and f <1 kHz. This is an

effect of the formerly identified shear layer, where the development of larger energy containing structures were shown in Figs 3 to 5. The increase in the high frequency energy content in the near wall region may be driven by the flow reattachment that results in the development of a turbulent boundary layer. After the reattachment, the development of the near-wall small-scale higher frequency related vortices are more significant, shown in Fig. 6 as area of increased $\Delta\phi_{uu}$. Based on the results presented in Fig. 4 to 6, one can conclude that after the reattachment point, the development of turbulent structures are significant in two regions, low frequency related vortices developed in the shear layer and high frequency related vortices developed in the near-wall region.

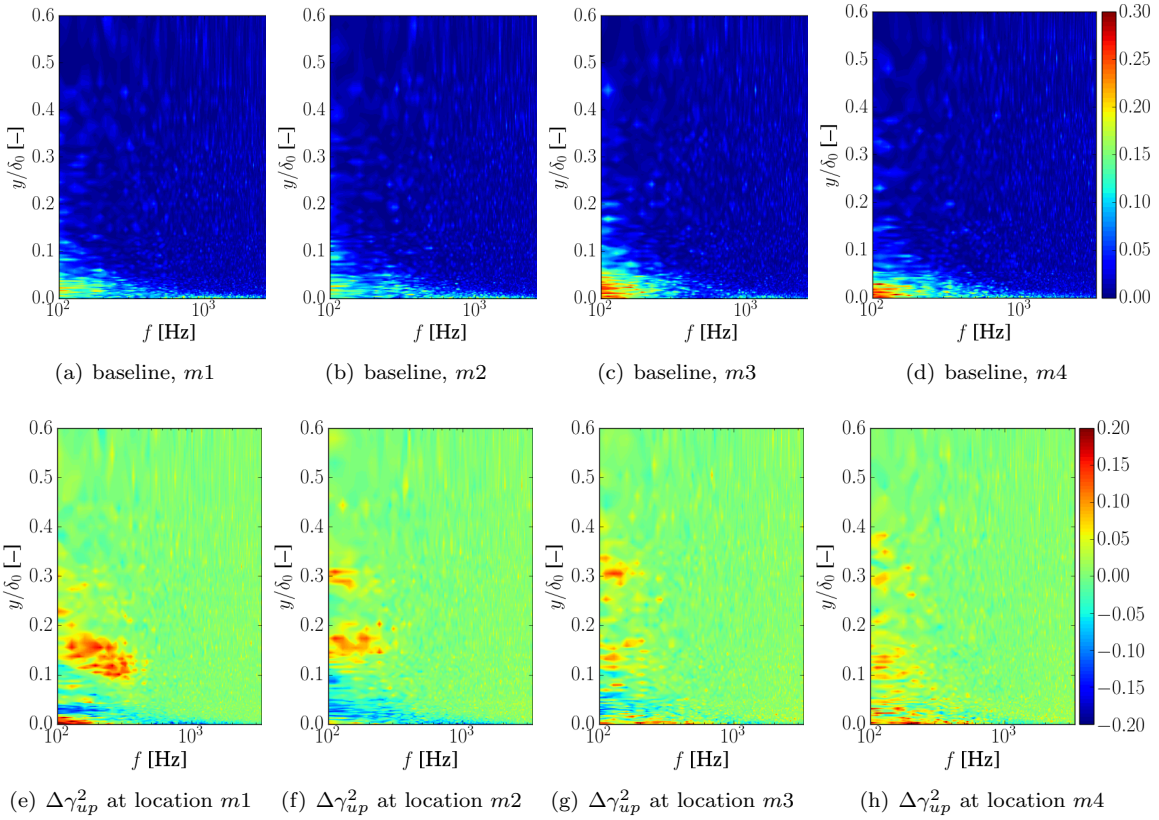

(a) baseline, $m1$ (b) baseline, $m2$ (c) baseline, $m3$ (d) baseline, $m4$

(e) $\Delta\gamma^2_{up}$ at location $m1$ (f) $\Delta\gamma^2_{up}$ at location $m2$ (g) $\Delta\gamma^2_{up}$ at location $m3$ (h) $\Delta\gamma^2_{up}$ at location $m4$

Figure 7. Baseline results and change in the coherence (γ^2_{up}) in the boundary layer downstream of the active flow control section at locations $m1 - m4$ for the $\sigma = 0.22$ blowing flow control case

In order to better understand the link between the main driving components of the generated TE noise, i.e the surface pressure fluctuations, and the velocity fluctuations, the coherence (γ^2) between the measured microphone and hot-wire signals has been investigated. This can help the better understanding of the contribution of velocity fluctuations to the surface exerted pressure fluctuations in the frequency domain. Figure 7 shows the baseline (no AFC) γ^2 (Fig. 7 (a) to (d)) and the changes (Fig. 7 (e) to (h)) in the measured coherence at locations $m1 - m4$ ($\Delta\gamma^2_{up} = \gamma^2_{up,\text{AFC}} - \gamma^2_{up,\text{Baseline}}$ [–]). The newly introduced flow (below $y/\delta_0 \approx 0.2$) at the location $m1$ in Fig. 7(e) splits up the figure into three regions along the y-axis. There is an increase in the coherence very close to the wall, above which an area of decreased $\Delta\gamma^2_{pu}$ can be observed followed by an area of increased $\Delta\gamma^2_{up}$ further away from the surface. The location of these changes coincides with the double peaks experienced in the u_{rms} profiles above $m1$ (see Fig. 5). The separation in this case is indicated by the layered structure of γ^2_{up}. The decrease experienced at $m1$ is due to the low energy content injected flow, while the increase above $y/\delta_0 \approx 0.1$ is associated with the presence of the shear layer developed above the newly introduced fluid layer. The reduction in $\Delta\gamma^2_{up}$ fades away and turns into an increase further downstream, indicating that the velocity fluctuations in the wall-normal area are of $y/\delta_0 = 0 - 0.3$ playing a more significant role in the exerted surface pressure fluctuations.

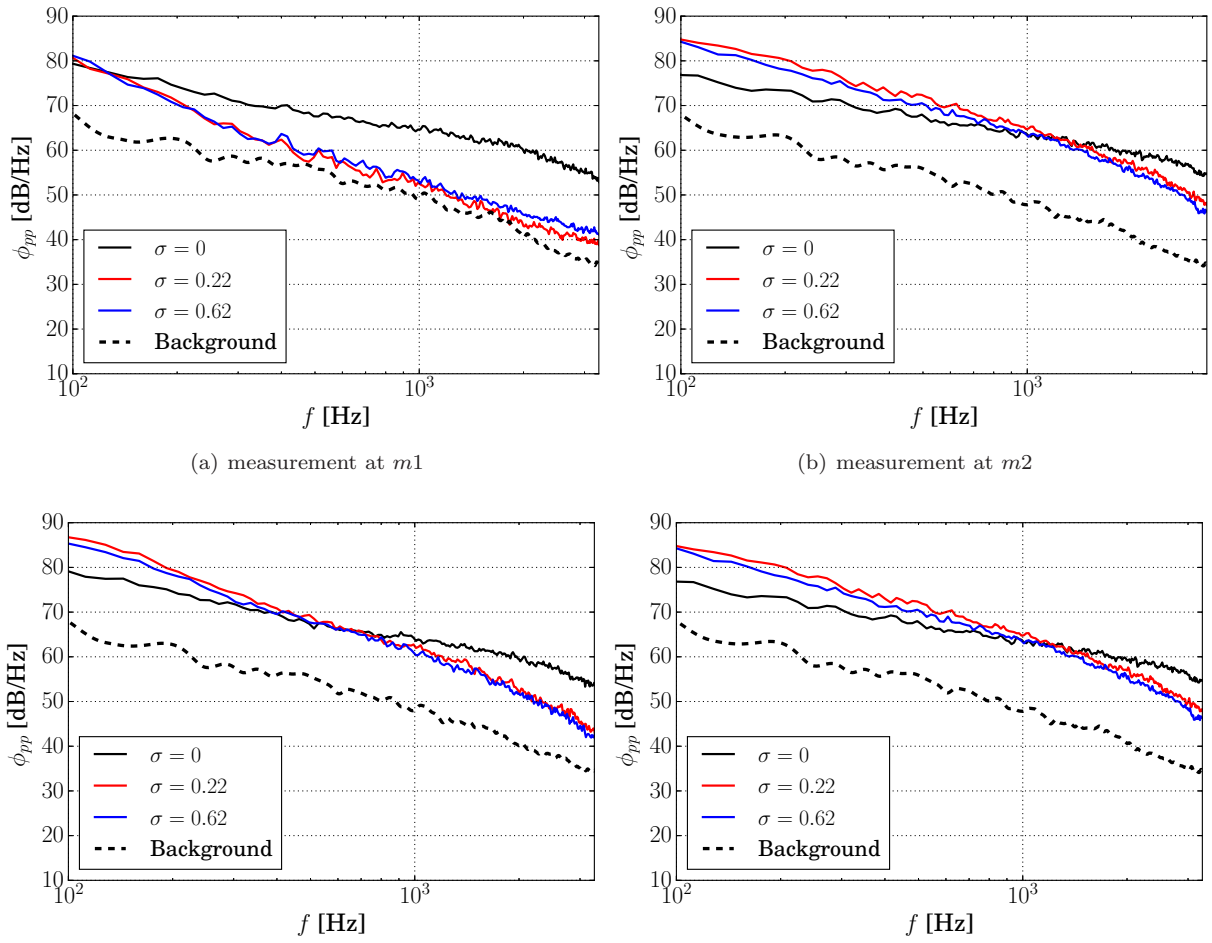

(a) measurement at $m1$

(b) measurement at $m2$

(c) measurement at $m3$

(d) measurement at $m4$

Figure 8. Surface pressure fluctuation spectra ϕ_{pp} downstream of the active flow control section at locations $m1 - m4$ for the blowing flow control cases

Figure 8 shows the effect of blowing on the surface pressure fluctuations (ϕ_{pp}) at the locations $m1$-$m4$. The AFC has a clear visible broadband effect on the measured spectra. Downstream of the flow control section, at the location $m1$, a significant broadband reduction of up to 10 dB/Hz in ϕ_{pp} is observed. This is originated from the previously seen complex effect of blowing, such as shifting the energy containing eddies farther away from the wall, while reducing their contribution to the surface pressure fluctuations and introducing a lower energy containing fluid layer close to the wall. As we approach the TE, the reduction in ϕ_{pp} is less significant due to the development of the shear layer, as shown in Fig. 3. An increase in the the lower frequency region is experienced further downstream, which is also originated from the development of a shear layer.

The previously presented results suggest that in order to maximize the TE noise reduction benefit of the system, the AFC treatment should be located close to the TE. To get a better estimate of the ideal location of the AFC, the changes in the surface pressure fluctuations is plotted in Fig. 9 ($\Delta\phi_{pp}(x,f) = \phi_{pp,\mathrm{AFC}} - \phi_{p,\mathrm{Baseline}}$ [dB/Hz]) as a function of the streamwise coordinate (x/δ_0) and frequency. The dashed lines represent the $m1$-$m4$ locations, and the zero level shown by a black contour line. In accordance with the findings in Fig. 8, the results show that the blowing can significantly reduce the surface pressure fluctuations shortly downstream of the AFC section. It can be seen that for the current AFC method, the TE should be in the vicinity of the AFC section to fully exploit the reduction in the measured surface pressure fluctuations. At this location, the ϕ_{pp} energy reduction is still reasonably high and the effects of energy containing structures within the shear layer is not yet felt on the surface.

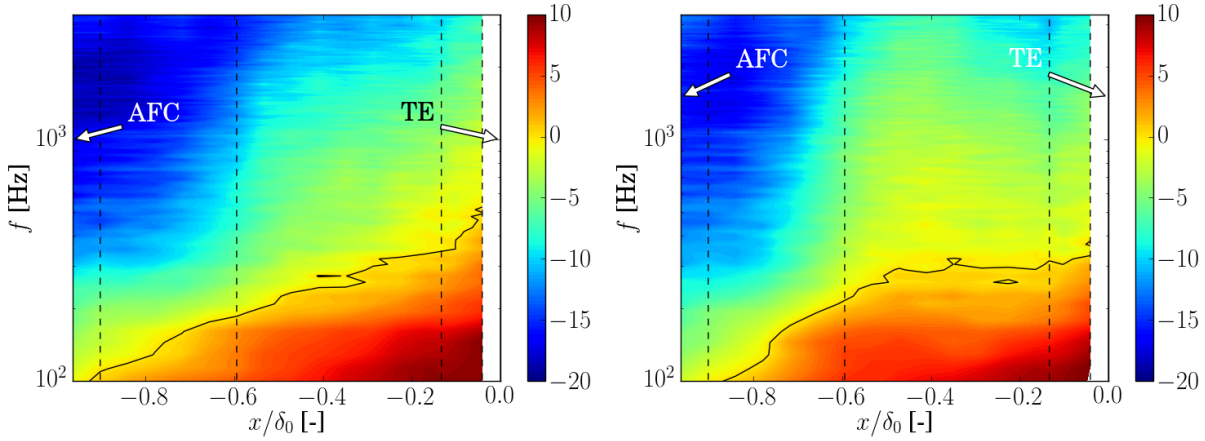

(a) $\sigma = 0.22$ (b) $\sigma = 0.62$

Figure 9. Change in the surface pressure fluctuation spectra $\Delta\phi_{pp}(x,f)$ downstream of the active flow control section for the $\sigma = 0.22$ and $\sigma = 0.62$ blowing flow control cases

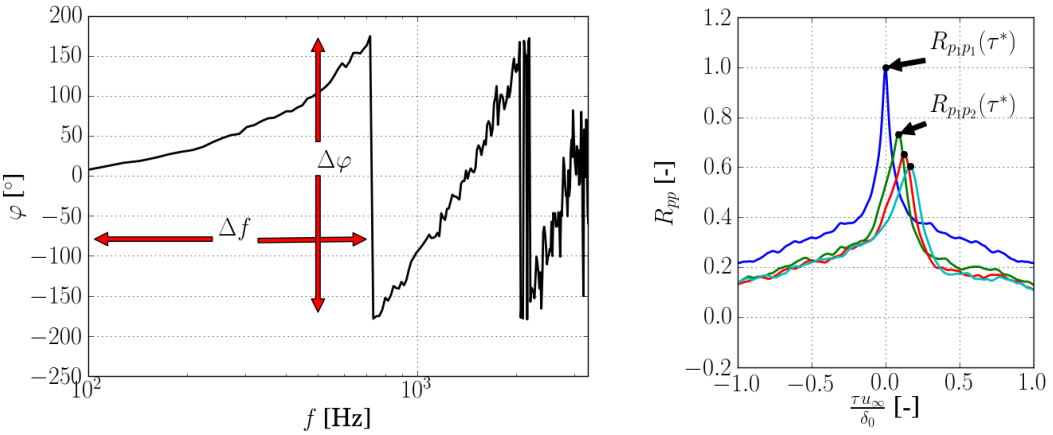

(a) Convection velocity measurement with phase shift between microphone signals

(b) Convection velocity measurement with cross-correlation between microphone signals

Figure 10. Measurement of the convection velocity

The convection velocity, which is also an important input parameter of Amiet's TE noise model, has been measured downstream of the AFC section using the streamwise microphones. The convection velocity can be calculated using two methods: (a) the phase shift calculated from the cross-spectra of two streamwise microphones (see Eq. (3) and Fig. 10(a)), and (b) the corresponding phase lag associated to the peaks of the

temporal cross-correlation of two streamwise microphones (see Eq. (4) and Fig. 10(b))

$$u_c = \frac{2\pi \Delta f \Delta x}{\Delta \varphi}, \tag{3}$$

$$u_c = \frac{\Delta x}{\tau^*}. \tag{4}$$

The calculated convection velocities are listed in Table 3. The calculation was not successful for $m1$ in the case of applied AFC, indicating the presence of flow separation and that the presenting structures were not strong enough to leave a significant pattern on the microphone signals. The phase shift based method was resulting in a generally lower u_c values than the cross-correlation method. Results have shown that the use of blowing resulted in the reduction of the convection velocity, which is in agreement with the momentum deficit results previously seen in Fig. 4. It is also clear from the results that the convection velocity decreases with increasing the blowing rate (σ).

Table 3. Measured convection velocities at locations $m1$ and $m4$ for the different perpendicular blowing rates (based on τ^*: temporal cross-correlation approach, based on Δf: cross-spectra approach)

u_c/u_∞ [−]	$m1$		$m4$	
Blowing rates	based on τ^*	based on Δf	based on τ^*	based on Δf
$\sigma = 0$	0.536	0.474	0.685	0.659
$\sigma = 0.22$	0.421	–	0.602	0.428
$\sigma = 0.62$	0.324	–	0.517	0.441

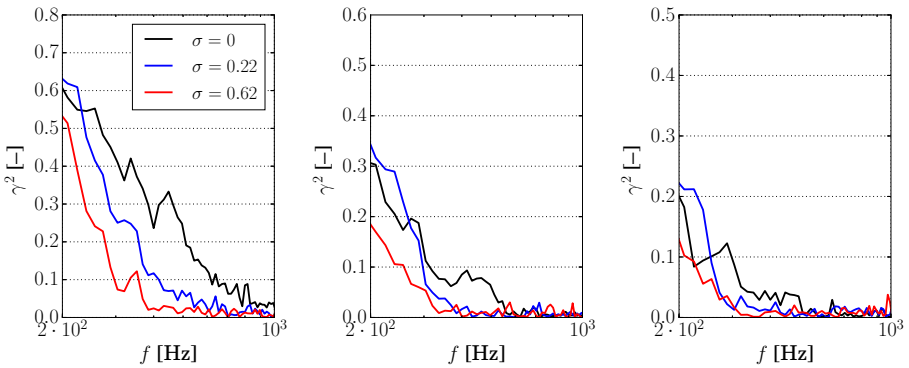

(a) $\Delta x = 3.6$ mm (b) $\Delta x = 7.8$ mm (c) $\Delta x = 11.4$ mm

Figure 11. Spanwise coherence for the perpendicular blowing AFC methods

Another important parameter in Amiet's trailing edge noise model is the spanwise correlation length of the turbulent structures near the TE, which can be calculated using the coherence between the spanwise microphones near the TE. Figure 11 shows the changes in the spanwise coherence of microphone signals for the different blowing rates. It has been observed that the blowing can significantly reduce the coherence indicating the elimination of the coherent structures and the emergence of some new less coherent turbulent structures. As the spanwise coherence is an important parameter in the TE noise models, it can be concluded that its reduction will result in lower TE generated far-field noise.

B. Steady Uniform Inclined Blowing

The results in the previous section showed that perpendicular flow injection can lead to the boundary layer separation and some undesired effects. In order to reduce these effects, while maintaining the achieved reduction in the surface pressure fluctuations, an inclined blowing AFC method has been developed, capable of introducing flow at 30° incidence with respect to the x-axis as shown in Fig. 2.

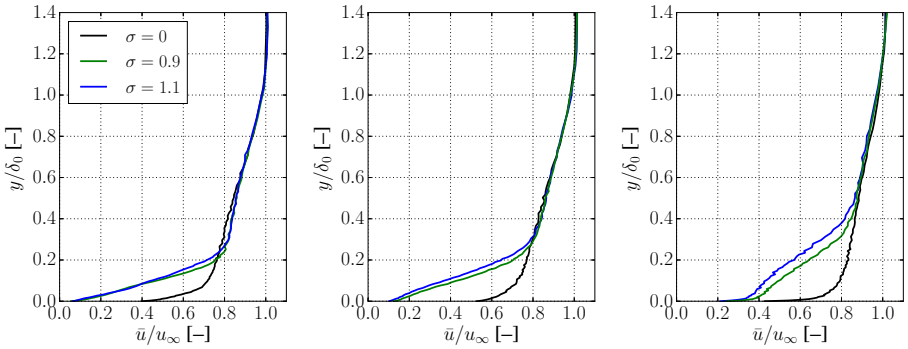

(a) $\overline{u}$ profiles at $m1$ (b) $\overline{u}$ profiles at $m2$ (c) $\overline{u}$ profiles at $m4$

Figure 12. Mean velocity profiles downstream of the active flow control section at locations $m1 - m4$ for the inclined blowing flow control cases

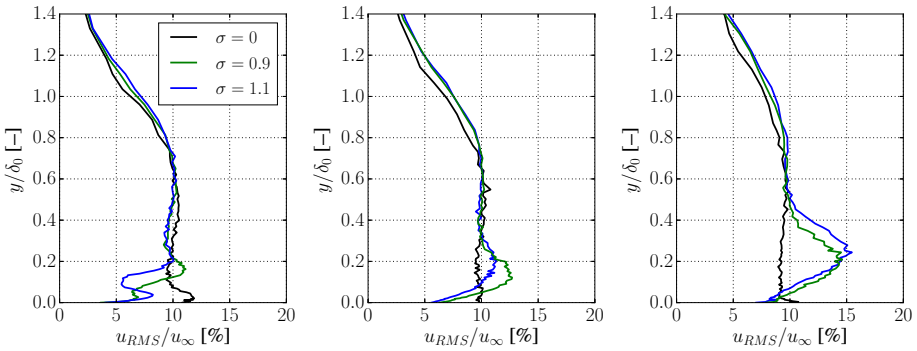

(a) u_{rms} profiles at $m1$ (b) u_{rms} profiles at $m2$ (c) u_{rms} profiles at $m4$

Figure 13. Root mean square velocity profiles downstream of the active flow control section at locations $m1 - m4$ for the inclined blowing flow control cases

As before, hot-wire measurements have been carried ot at the locations $m1$, $m2$ and $m4$ for the inclined blowing case. The mean velocity profiles are shown in Fig. 12. Comparing the results to the perpendicular blowing case, the first observation is that the inclined blowing does not result in significant velocity overshoot in the boundary layer. There is only a slight increase in the momentum at $m1$ between $y/\delta_0 = 0.2$-0.5, which is not observed at the downstream locations. The velocity profiles show no inflexion in the case of inclined blowing, suggesting the lack of flow separation. There is a significant momentum deficit close to the wall, which becomes more pronounced downstream.

The velocity root mean square profiles, measured using single component hot-wire, are shown in Fig. 13. The results of the $\sigma > 0$ cases at the location $m1$ show a complex flow structure. There is a significant reduction at location $m1$ in the presented rms profiles for $\sigma = 0.9$, while a slight overshoot for the $\sigma = 1.1$ case at $y = \delta_0 \approx 0.2$ has been observed. The amplitude of the second peak from the wall observed at $m1$ increases as the flow advances downstream. Similarly shaped velocity rms profiles were observed in the case of perpendicular blowing at $m4$, see Fig. 5. There is a lower amount of increase experienced in the velocity rms profiles at the outer regions of the BL compared to the normal blowing case.

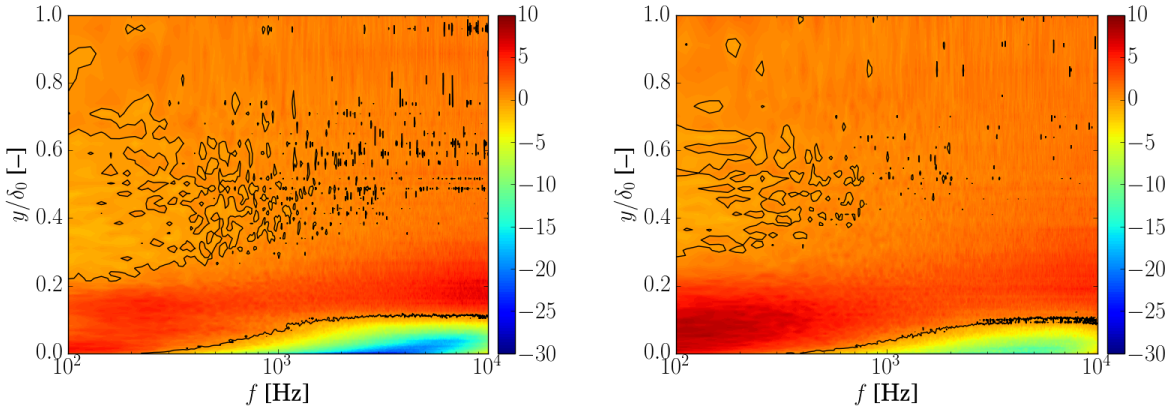

(a) measurement at $m1$

(b) measurement at $m2$

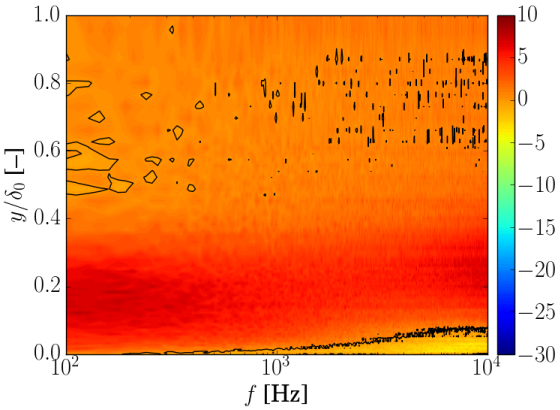

(c) measurement at $m4$

Figure 14. Change in the power spectra of the u velocity component within the boundary layer ($\Delta\phi_{uu}$ [dB/Hz]) downstream of the active flow control section at locations $m1 - m4$ for the $\sigma = 0.9$ inclined blowing flow control case

The change in the frequency-energy content ($\Delta\phi_{pp}$) of the streamwise velocity fluctuations within the boundary layer for the $\sigma = 0.9$ case is presented in Fig. 14. The trends are similar to those observed in Fig. 6 for the perpendicular blowing case. In the near-wall ($y/\delta_0 = 0 - 0.2$) and the high frequency ($f > 1$ kHz) region a significant reduction has been observed. Another region of energy reduction is found in $y/\delta_0 = 0.2 - 0.6$ below 1 kHz, which coincides with the area of the slight velocity overshoot shown in Fig. 12. An increase in the energy content between the two area is observed. The amplitude of both the ϕ_{pp} reduction and increase is lower in the inclined blowing case than for the perpendicular case.

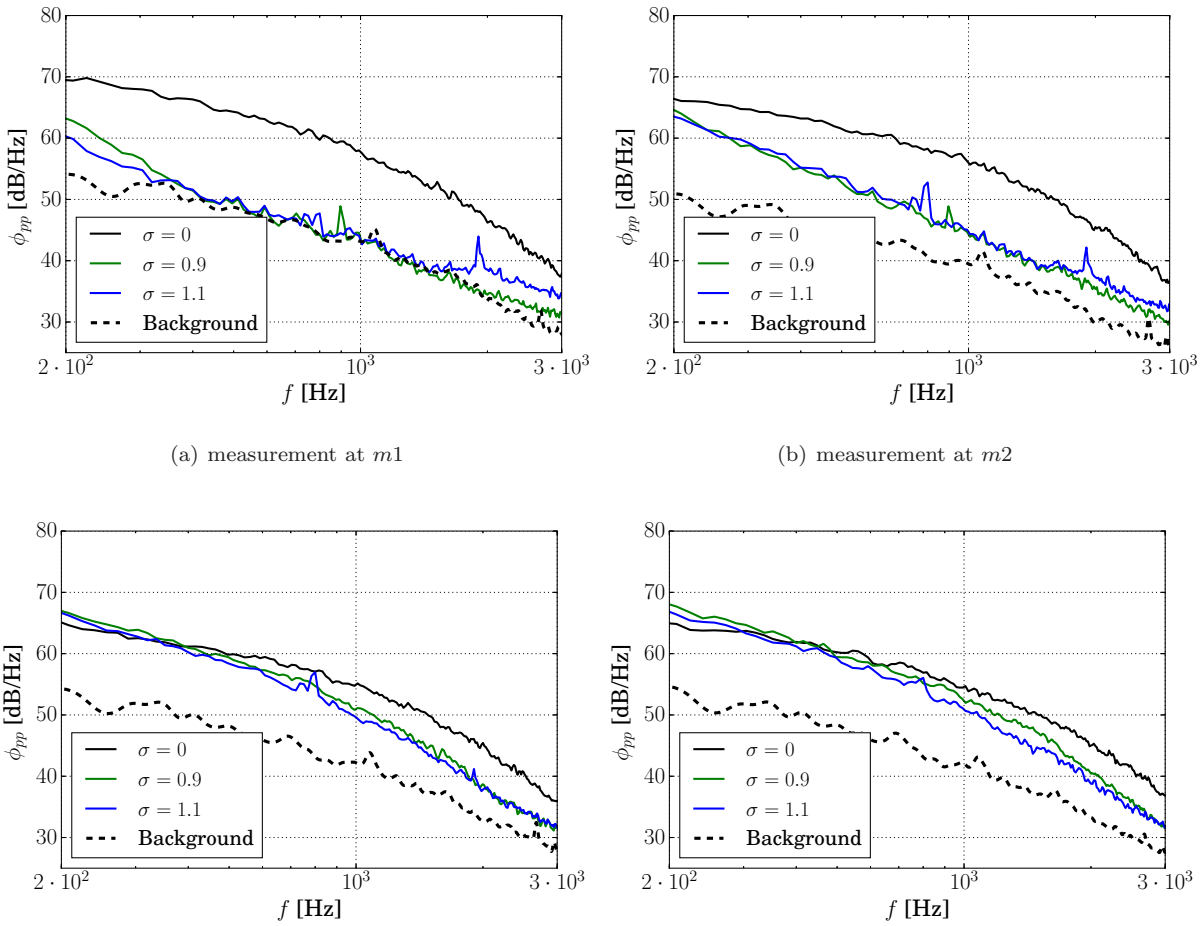

(a) measurement at $m1$

(b) measurement at $m2$

(c) measurement at $m3$

(d) measurement at $m4$

Figure 15. Surface pressure fluctuation spectra ϕ_{pp} downstream of the active flow control section at locations $m1 - m4$ for the inclined blowing flow control cases

The measured surface pressure fluctuations downstream of the inclined blowing is shown in Fig. 15. The applied treatment leads to a more significant reduction in the measured surface pressure spectra than the perpendicular blowing. At location $m1$, the spectra reached the background noise suggesting that significant reduction has been achieved. Quantitatively, the reduction was approximately 15 dB/Hz at location $m1$ slightly below 1 kHz. The achieved noise reduction is better conserved in this case than for the perpendicular treatment as the measured reduction in ϕ_{pp} is still approximately 10 dB/Hz at $m2$. The previously seen build-up of lower frequency pressure fluctuations is also observed in this case, but it is much less significant than in the perpendicular blowing case.

The inclined blowing, compared to the perpendicular blowing, can lead to a delayed increase in the low frequency noise component. Based on the results in Fig. 16, the treatment still needs to be located close to the TE to exploit its favourable effects on the surface pressure fluctuations. It is also visible in Fig. 16 that there is only a slight difference between the two presented blowing cases, and the lower σ was found to be slightly more effective in reducing ϕ_{pp} than the higher σ. The coherence between the spanwise microphone signals is presented in Fig. 17. Similarly to the perpendicular blowing case, a significant reduction in γ^2 has been observed over the whole frequency range of interest. This indicates an appreciable reduction in the coherence of the turbulent structures responsible for TE noise generation. The level of coherence reduction is found to be proportional to the applied blowing rate (σ).

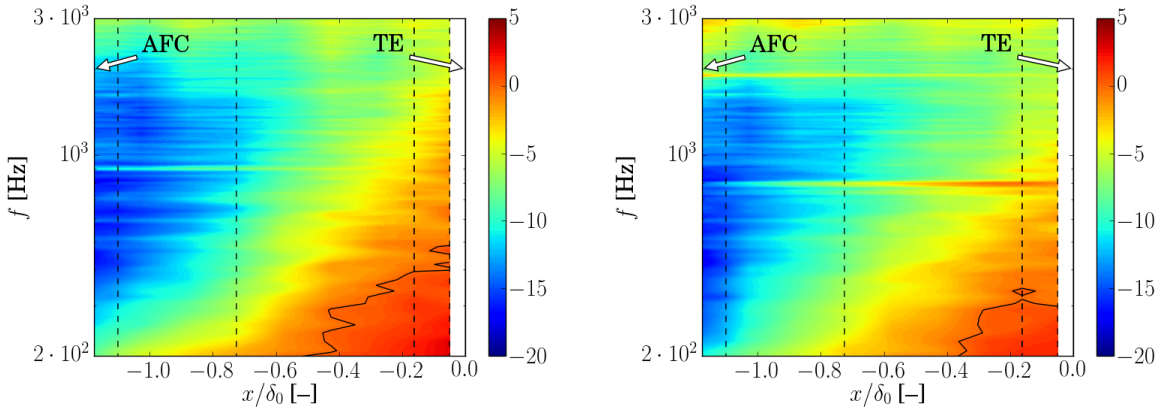

(a) $\sigma = 0.9$ (b) $\sigma = 1.1$

Figure 16. Change in the surface pressure fluctuation spectra $\Delta\phi_{pp}(x, f)$ downstream of the active flow control section for the inclined blowing flow control cases

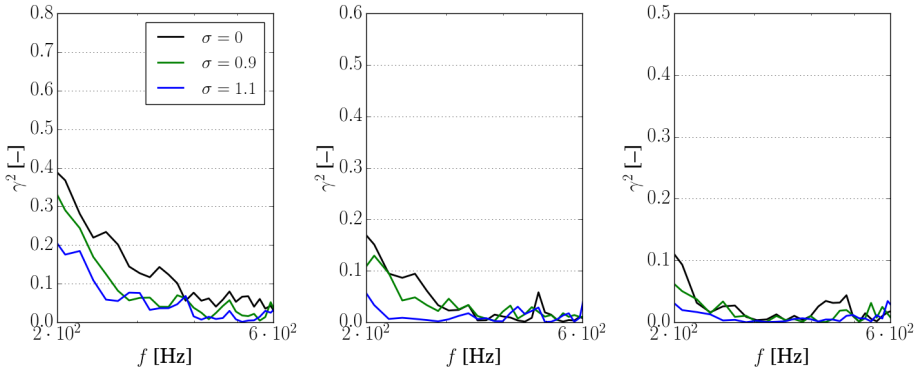

(a) $\Delta x = 3.6$ mm (b) $\Delta x = 7.8$ mm (c) $\Delta x = 11.4$ mm

Figure 17. Spanwise coherence for the inclined blowing AFC methods

Table 4. Boundary layer properties at locations $m1$ and $m4$ for the inclined blowing cases

	σ [–]	u_∞ [m/s]	δ [mm]	δ^* [mm]	θ [mm]	u_τ [m/s]	Re_θ [–]
$m1$	0	10	73.04	11.28	8.68	0.400	5,700
	0.9		75.06	14.11	8.54	0.395	5,800
	1.1		77.54	14.86	8.46	0.390	5,900
$m4$	0	10	72.86	8.03	6.66	0.425	5,600
	0.9		73.47	12.74	8.45	0.405	6,800
	1.1		74.22	14.55	8.98	0.400	6,100

C. Steady Uniform Perpendicular Suction

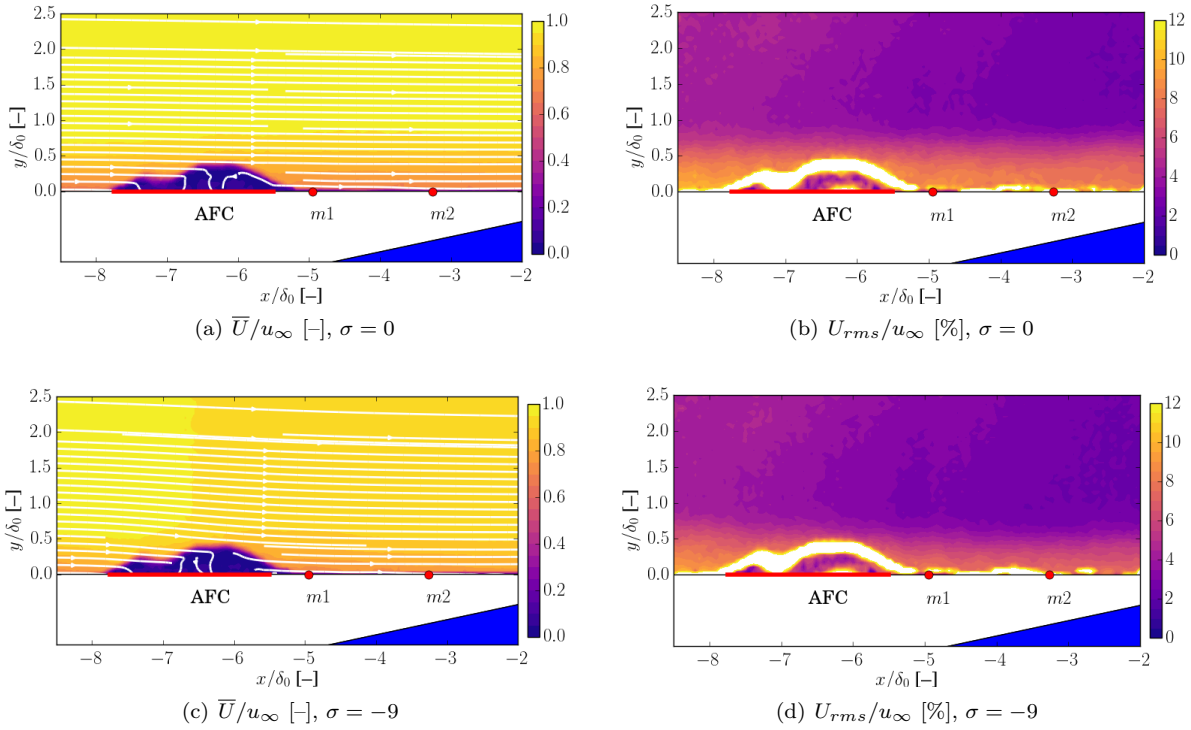

(a) $\overline{U}/u_\infty$ [–], $\sigma = 0$ (b) U_{rms}/u_∞ [%], $\sigma = 0$

(c) $\overline{U}/u_\infty$ [–], $\sigma = -9$ (d) U_{rms}/u_∞ [%], $\sigma = -9$

Figure 18. Velocity magnitude with streamlines (left column) and flow energy content in percent of free-stream velocity (right column) measured with the use of PIV downstream of the AFC section for the $\sigma = 0$ and $\sigma = -9$ suction cases

The use of flow suction for aeroacoustic purposes has been the subject of some recent studies.[39–41,43,44] In this section we shall study the effects of flow suction on the main quantities responsible of TE noise generation, namely, surface pressure fluctuations (ϕ_{pp}), convection velocity (u_c), lateral coherence (γ^2), etc. The PIV images presented in Fig. 18 reveal that the flow streamlines are brought closer to the wall after the use of flow suction and the velocity rms magnitude decreases downstream of the AFC section. This indicates that the application of flow suction results in the reduction of boundary layer size, which suggests that δ^* and θ is also reduced as a result of flow suction.

Table 5. Boundary layer properties at locations $m1$ and $m4$ for the perpendicular suction cases

	σ	u_∞	δ	δ^*	θ	u_τ	Re_θ
	[–]	[m/s]	[mm]	[mm]	[mm]	[m/s]	[–]
$m1$	0	10	20.66	2.51	1.79	0.485	1,200
	−3		29.01	2.49	2.12	0.480	1,430
	−9		51.03	3.47	3.10	0.475	2,100
$m4$	0	10	20.33	1.53	1.30	0.525	920
	−3		17.77	1.04	0.92	0.550	630
	−9		12.44	0.41	0.37	0.650	258

Figure 19 shows the BL mean velocity profiles measured using hot-wire anemometry. The suction affects the shear in the BL, especially at $m4$, by splitting it up into two distinct regions: a high velocity gradient region below $0.1\delta_0$ and a low velocity gradient region above this point. The boundary layer properties for locations $m1$ and $m4$ are listed in Table 5 with and without flow suction. The boundary layer thickness is more significantly affected for this treatment than for the blowing cases. The results in Table 5 indicates that the BL thickness increases right after the AFC location and as the flow advances downstream, the boundary layer thickness decreases to $\delta \approx 0.6 - 0.7\delta_0$, where δ_0 is the BL thickness for $\sigma = 0$. This is shown in Fig. 19(a) by the fact that the treated profiles do not reach the free-stream velocity even at $1.4\delta_0$, indicating an increased BL thickness. Similar findings were observed by Park and Choi,[35] where a jump in the boundary layer momentum thickness was reported just downstream of the AFC slit, followed by a decrease further downstream. The boundary layer momentum thickness (θ) has been significantly reduced for the $\sigma = -9$ case by 70 % of its original value due to the increase of velocity magnitude within in the BL.

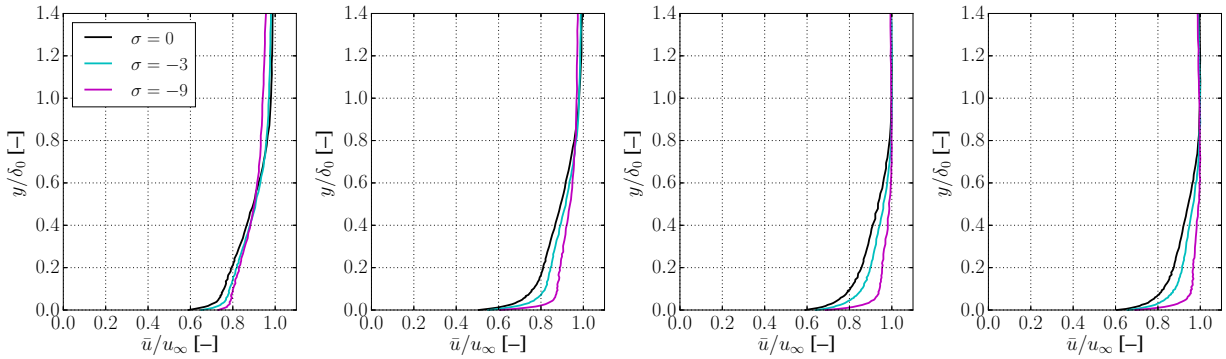

(a) $\overline{u}$ profiles at $m1$ (b) $\overline{u}$ profiles at $m2$ (c) $\overline{u}$ profiles at $m3$ (d) $\overline{u}$ profiles at $m4$

Figure 19. Mean velocity profiles downstream of the active flow control section at locations $m1 - m4$ for the suction flow control cases

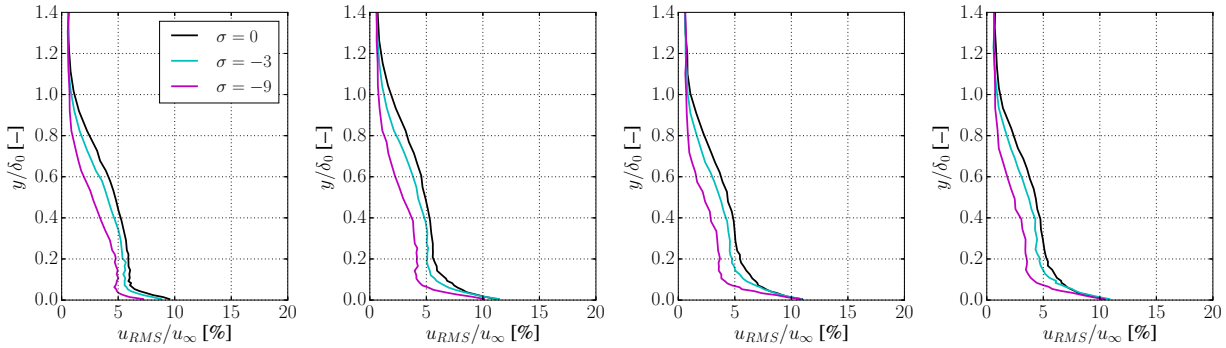

(a) u_{rms} profiles at $m1$ (b) u_{rms} profiles at $m2$ (c) u_{rms} profiles at $m3$ (d) u_{rms} profiles at $m4$

Figure 20. Root mean square velocity profiles downstream of the active flow control section at locations $m1 - m4$ for the suction flow control cases

The velocity rms results are presented in Fig. 20. A significant reduction in the flow energy content is observed over the entire BL for all locations. It is not visible from Fig. 20 whether flow laminarization was achieved, hence further hot-wire and hot-film measurements are planned to find the suction rate required for full flow laminarization. The distance between the AFC section and the TE covers a distance of $5\delta_0$ and the results have shown that even in the case of modest flow suction, the flow does not recover to that of the baseline ($\sigma = 0$) case within this distance. This is in agreement with the findings of Antonia *et al.*,[34] who reported that for $\sigma = -2.6$ the flow requires approximately $40\delta_0$ to return to its original state ($x = 0$, $\sigma = 0$). The treated profiles partially return to their original values in the near-wall region beyond the locations $m2$ and $m4$, which agrees with the findings of Park and Choi[35] and Antonia *et al.*,[34] where the near-wall energy content of the streamwise velocity component was shown to return to its original value in

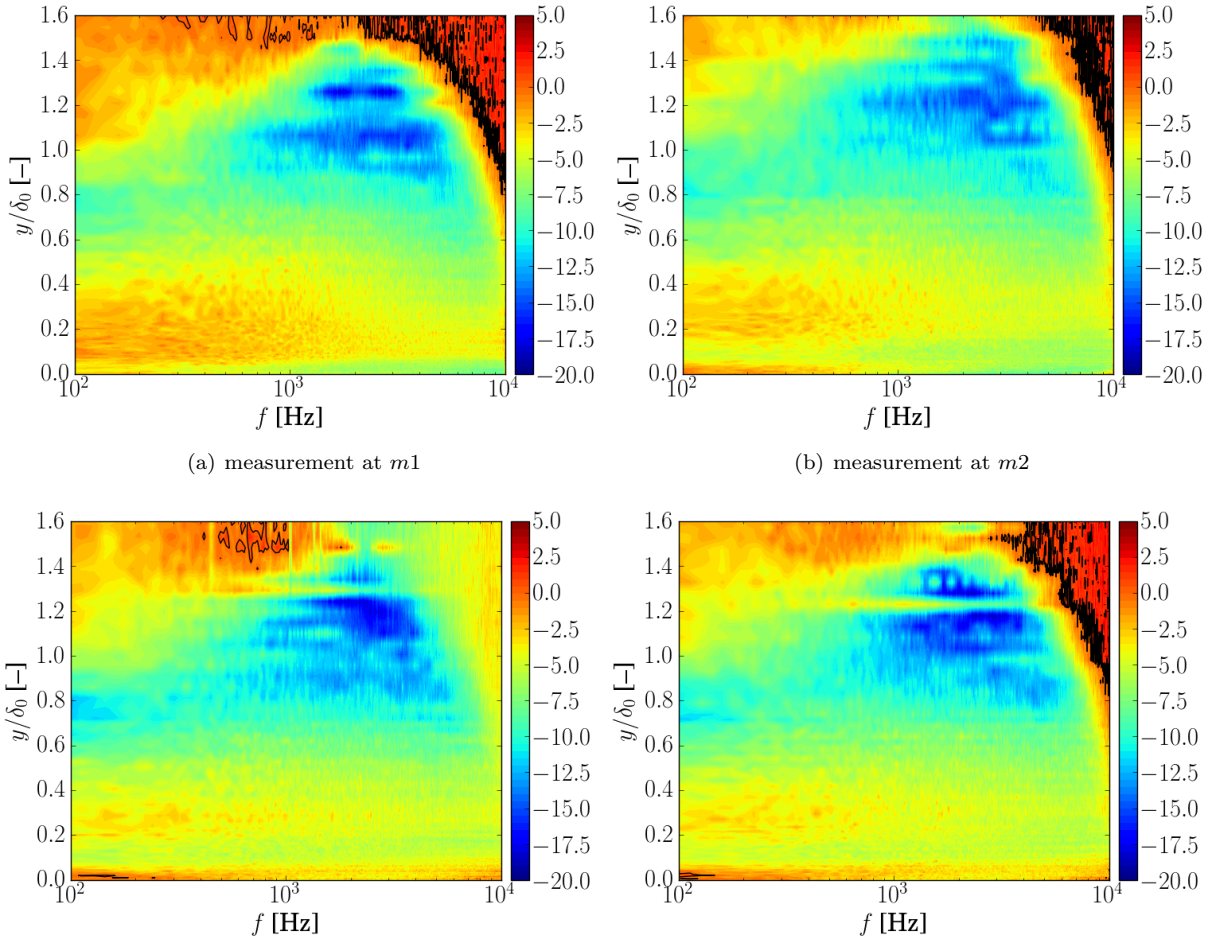

(a) measurement at $m1$

(b) measurement at $m2$

(c) measurement at $m3$

(d) measurement at $m4$

Figure 21. Change in the power spectra of the u velocity component within the boundary layer ($\Delta\phi_{uu}$ [dB/Hz]) downstream of the active flow control section at locations $m1 - m4$ for the $\sigma = -9$ suction flow control case

near-wall energy content of the streamwise velocity component was shown to return to its original value in a short distance. The study also reported that as the turbulent structures were brought closer to the wall, the viscous dissipation increased downstream of the AFC treatment. This effect is going to be investigated with the help of additional PIV measurements.

Figure 21 shows the observed changes in the frequency-energy content of the u velocity component along the boundary layer ($\Delta\phi_{uu}$ [dB/Hz]) for the $\sigma = -9$ case. The flow suction results in a broadband reduction of the streamwise energy content within the entire presented domain at all locations. The reduction is most pronounced at the edge of the BL. An important observation of the presented plots is hidden in their similarity. This indicates that the achieved reduction remains approximately constant both in terms of amplitude and shape, unlike in the blowing case, where significant changes took place downstream of the AFC section in the flow. The amount of reduction observed at location $m1$ (Fig. 21(a)) below $0.4\delta_0$ is less significant, but this becomes more pronounced in the same area further downstream. This might be the indication of the increase in the viscous dissipation that reduces the amount of turbulent structures present in the flow. The reduction achieved closer to the wall (below $0.1\delta_0$) fades away downstream, in accordance with the rms results in Fig. 20, which can be due wall induced turbulent structures. Additional PIV measurements are planned to further investigate these observations.

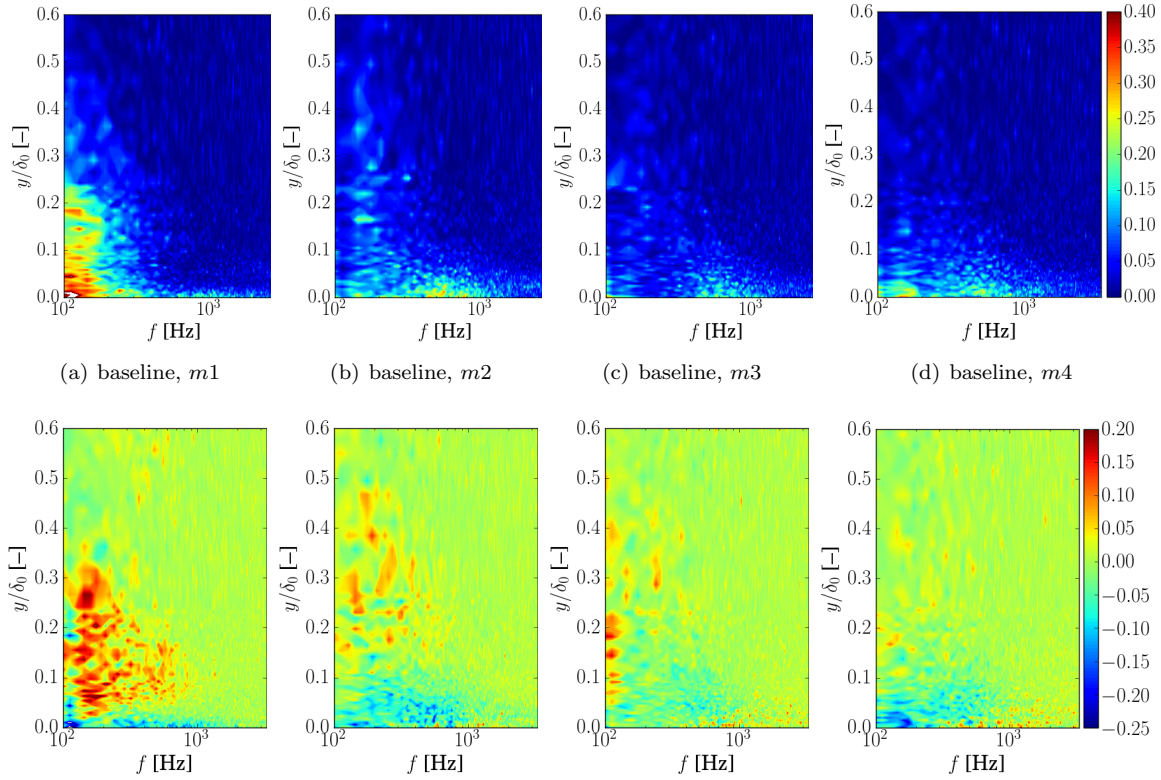

(a) baseline, $m1$ (b) baseline, $m2$ (c) baseline, $m3$ (d) baseline, $m4$

(e) $\Delta\gamma^2_{up}$ at location $m1$ (f) $\Delta\gamma^2_{up}$ at location $m2$ (g) $\Delta\gamma^2_{up}$ at location $m3$ (h) $\Delta\gamma^2_{up}$ at location $m4$

Figure 22. Baseline results and change in the coherence (γ^2_{up}) in the boundary layer downstream of the active flow control section at locations $m1 - m4$ for the $\sigma = -9$ suction flow control case

The coherence between the measured surface pressure fluctuations and streamwise velocity component is shown in Fig. 22. The figure shows the coherence for the baseline (Fig. 22 (a)-(d)) and the observed changes with respect to the baseline for the $\sigma = -9$ suction case (Fig. 22 (e)-(h)). Results have shown a high coherence near the wall and at low frequencies for the first location ($m1$) in the baseline case (Fig. 22 (a)), which is associated with the perturbation on the flow caused by the surface condition of the applied AFC system. An increase in $\Delta\gamma^2_{up}$ was observed for the $\sigma = -9$ case at the same $m1$ location. This might be an effect of turbulent structures being brought closer to the wall due to suction, and therefore an increase in their contribution to the measured surface pressure fluctuation. Further downstream of location $m1$, a decrease in $\Delta\gamma^2_{up}$ below $y/\delta_0 = 0.1$ is observed, indicating that the coherence is nearly eliminated between the surface pressure and velocity fluctuations. The proper understanding of this phenomenon requires more in-depth studies and high quality PIV and hot-wire measurements.

The effect of the flow control suction on the surface pressure fluctuations downstream of the AFC section at locations $m1 - m4$ is presented in Fig. 23. In agreement with the results presented Figs. 19, 20and 22, where reduction in the energy content and coherence was observed, a broadband reduction is achieved in the ϕ_{pp} plots. Just downstream of the AFC, there is a slight increase at the low frequencies in the measured pressure spectra, but as the flow advances downstream, this fades away. We can see an approximately 8 dB reduction in the mid frequency region at the first location for $\sigma = -9$ (Fig. 23(a)). This reduction decreases and it spreads to the lower frequencies further downstream. The discussion presented for Fig. 21 on the flow behaviour downstream of the AFC can be brought in relation with the measured surface pressure spectra. It was shown by the ϕ_{uu} plots that the reduction at high frequency is higher closer to the AFC region and alongside with this, there was lower reduction (or even increase) at lower frequencies at $m1$ in the ϕ_{uu} plots. As we move toward the TE, the high frequency reduction begins to fade away (see Fig. 21(d)), but amplitudes at lower frequencies show further decrease. The same effects were found in the u_{rms}, $\Delta\phi_{uu}$ and $\Delta\gamma^2$ plots. Downstream of $m1$, the reduction in lower frequencies becomes more pronounced, while there is

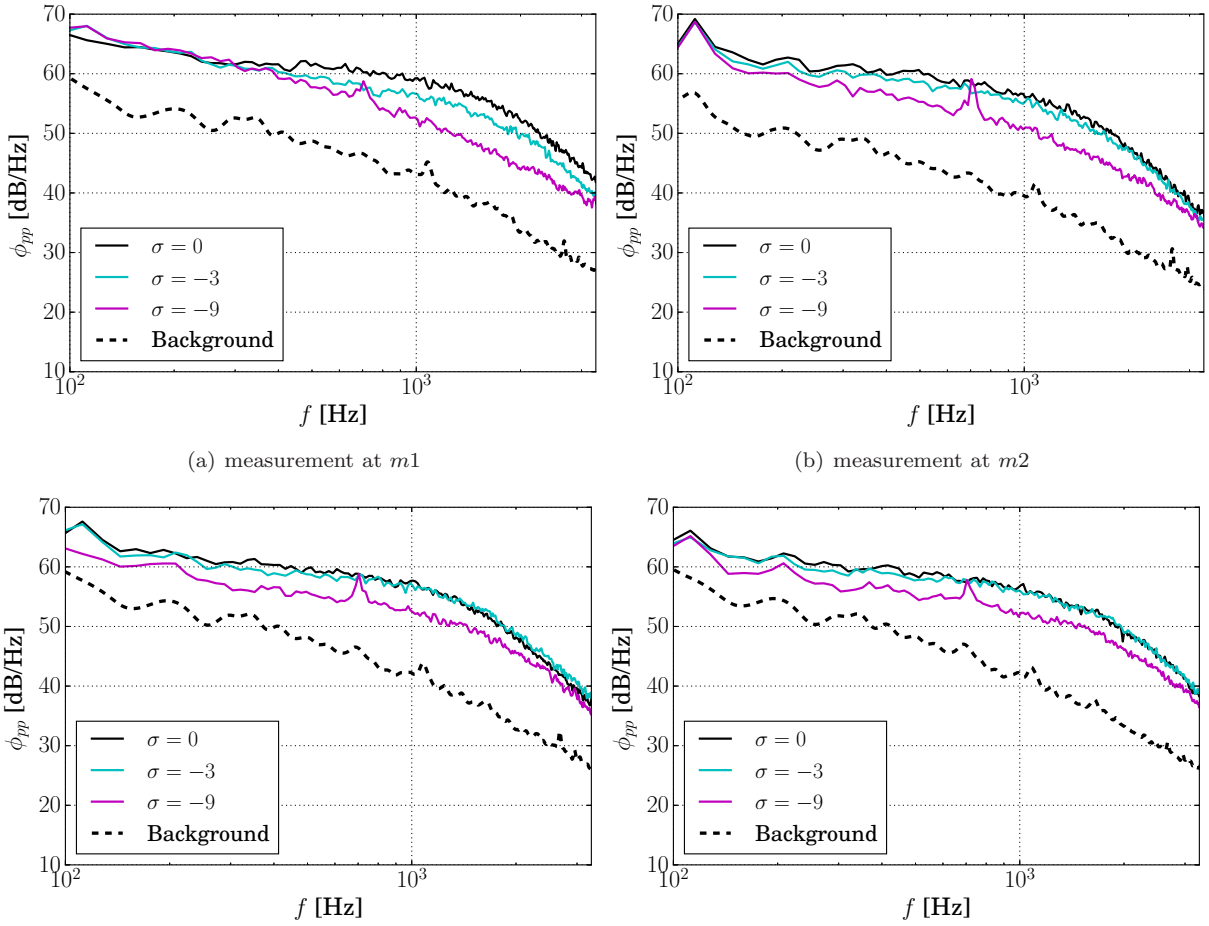

(a) measurement at $m1$

(b) measurement at $m2$

(c) measurement at $m3$

(d) measurement at $m4$

Figure 23. The measured surface pressure fluctuations (ϕ_{pp} [dB/Hz]) in the boundary layer downstream of the active flow control section at locations $m1 - m4$ for the suction flow control cases

section, which was reported by Park and Choi.[35]

The changes in the surface pressure spectra along the streamwise direction downstream of the AFC region for the $\sigma = -9$ case are presented in Fig. 24. An area of ϕ_{pp} increase is observed at low frequencies, separated by the black zero level contour line in the lower left corner. The energy increase disappears quickly by approximately $1.0\delta_0$ downstream of the AFC section. The figure indicates that the suction, in contrary to the of the blowing case, should be placed a few boundary layer distances upstream of the TE in order to ensure that significant reduction of the surface pressure fluctuations can be achieved.

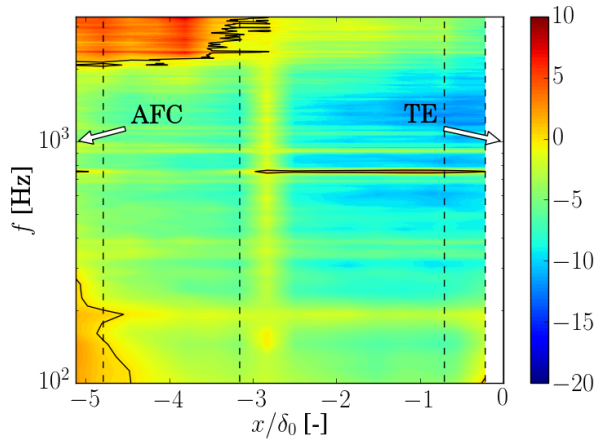

Figure 24. Change in the surface pressure fluctuation spectra ($\Delta\phi_{pp}(x, f)$) downstream of the active flow control section for the $\sigma = -9$ suction flow control case

The effect of the implementation of AFC system on the convection velocity was assessed using the same phase-shift and cross-correlation based techniques as discussed in the perpendicular blowing case. The result of these two methods are presented in Fig. 25. For the lower suction flow rate case it was possible to calculate the convection velocity but for the higher suction rate the methods failed to give reliable results. We can see that the phase jump based method generally underestimates the convection velocity, but the trends found by the two methods are the same. In contrary to the blowing case, the convection velocity increases as a result of the applied suction. This is in agreement with the findings of Fig. 19 and the measured thinner momentum thickness. One can interpret that the higher momentum containing BL passing over the surface is resulting in an increased convection velocity.

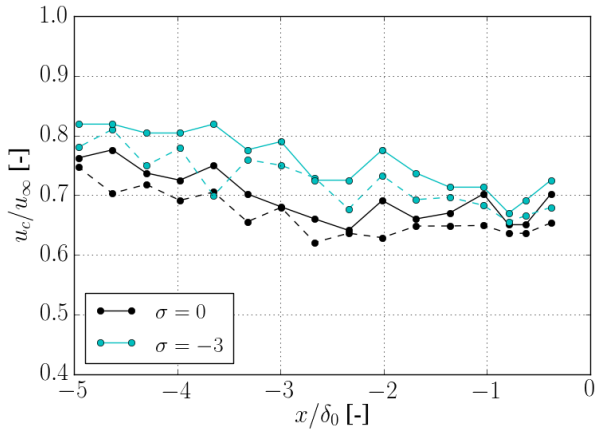

Figure 25. The measured convection velocities at different streamwise locations downstream of the flow control section for the suction cases, (dashed lines: cross-spectra based method, solid lines: cross-correlation based method)

The spanwise coherence of the pressure transducers in the vicinity of the TE is shown in Fig. 26. The coherence in the case of the low suction rate shows a slight increase, while that for the high suction rate has been significantly increased. The experienced increase for the $\sigma = -9$ case can be an indication of flow laminarization and the presence of two-dimensional coherent turbulent structures associated with laminar two-dimensional flow.

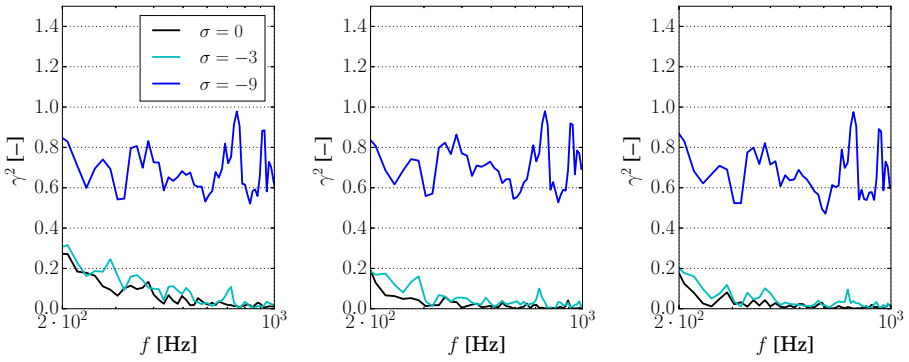

(a) $\Delta x = 3.6$ mm (b) $\Delta x = 7.8$ mm (c) $\Delta x = 11.4$ mm

Figure 26. Spanwise coherence for the perpendicular suction AFC methods

D. Steady Uniform Inclined Suction

It was anticipated that by inclining the direction of flow suction, as shown in Fig. 2, it can further improve the performance of the AFC system. The flow suction has been applied at an angle of 30° enabling the flow to smoothly enter into the AFC system.

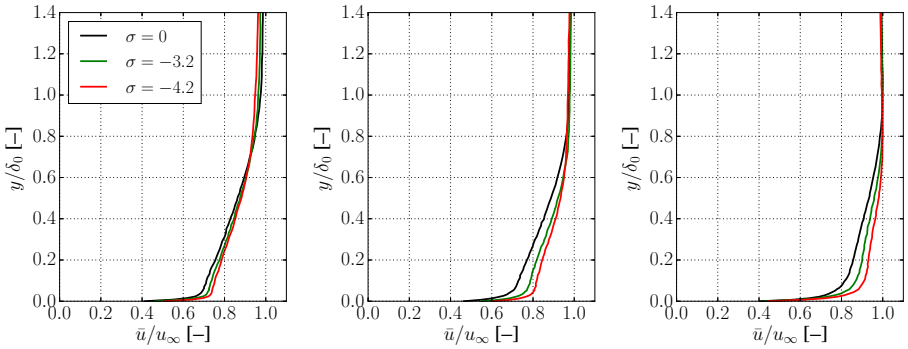

(a) $\overline{u}$ profiles at $m1$ (b) $\overline{u}$ profiles at $m2$ (c) $\overline{u}$ profiles at $m4$

Figure 27. Mean velocity profiles downstream of the active flow control section at locations $m1 - m4$ for the inclined suction flow control cases

Figure 27 shows the mean streamwise velocity component at the $m1$-$m4$ locations. It is visible that the inclined suction has the same effect on the measured BL profiles as the perpendicular treatment. At the first location ($m1$), a reduction in $\overline{u}$ at the outer BL is observed, indicating increase in the BL thickness. Further downstream, there is an increase in the velocity magnitude within the boundary layer resulting in the reduction of the momentum thickness, similar to the perpendicular suction case.

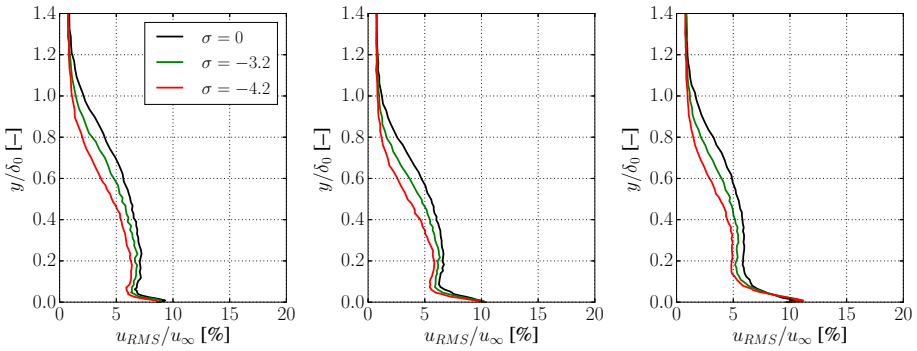

(a) u_{rms} profiles at $m1$ (b) u_{rms} profiles at $m2$ (c) u_{rms} profiles at $m4$

Figure 28. Root mean square velocity profiles downstream of the active flow control section at locations $m1 - m4$ for the inclined suction flow control cases

Significant reduction in the velocity rms values are observed within the entire boundary layer at all presented locations, see Fig. 28. The achieved reduction is approximately uniform along the BL and proportional to the applied suction rate. The near-wall ($y/\delta_0 < 0.1$) velocity rms values recover shortly downstream in this case, similar to the normal suction case.

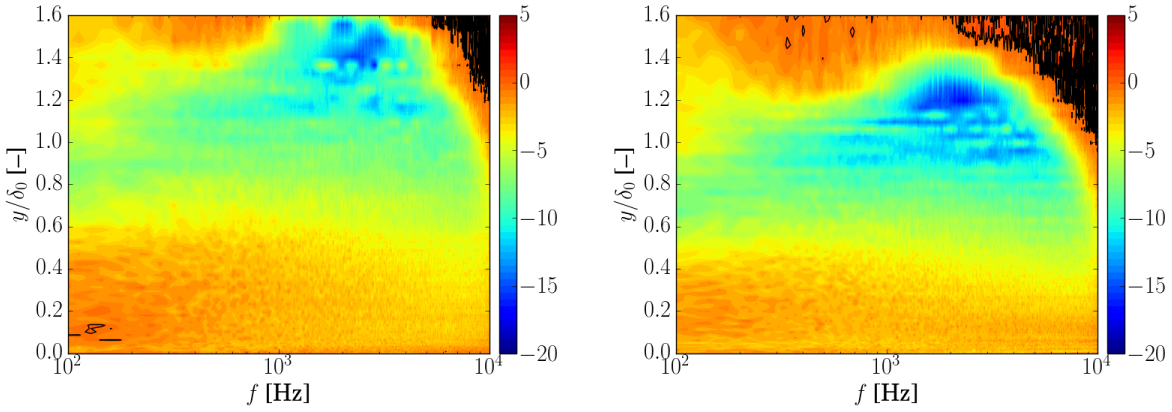

(a) measurement at $m1$

(b) measurement at $m2$

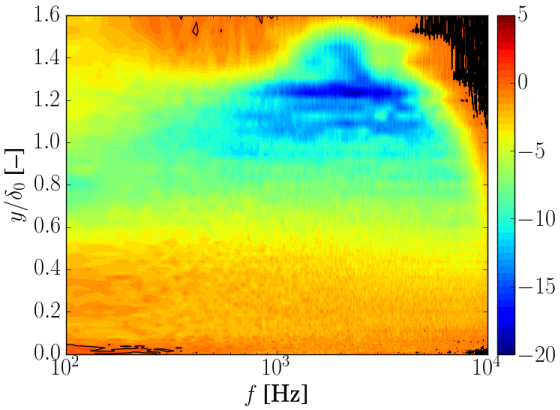

(c) measurement at $m4$

Figure 29. Change in the power spectra of the u velocity component within the boundary layer ($\Delta\phi_{uu}$ [dB/Hz]) downstream of the active flow control section at locations $m1 - m4$ for the $\sigma = -4.2$ inclined suction flow control case

The energy spectra of the streamwise velocity fluctuations along the boundary layer at the $m1 - m4$ locations is shown in Fig. 29. Similar observations can be made as in the perpendicular suction case. The flow suction resulted in a significant reduction in ϕ_{uu} within the entire boundary layer, and this is more pronounced in the outer part of the BL and at high frequencies. The achieved energy reduction does not change significantly at different locations indicating that the inclined suction can lead to a stable reduction in ϕ_{uu} along the streamwise coordinate.

The measured surface pressure fluctuation spectra at locations $m1 - m4$ is presented in Fig. 30. Similarly to the perpendicular suction case, a uniform reduction is observed in the entire presented frequency domain. The tonal peaks at around 700 Hz is originated from the AFC fan system. The largest reduction is approximately 8 dB/Hz slightly below 1 kHz. The shape of the curves is roughly the same in the presented locations, confirming that the change is almost independent of the location and the recovery to the original state is slow. This indicates that the applied treatment has a significant stabilizing effect on the achieved noise reduction.

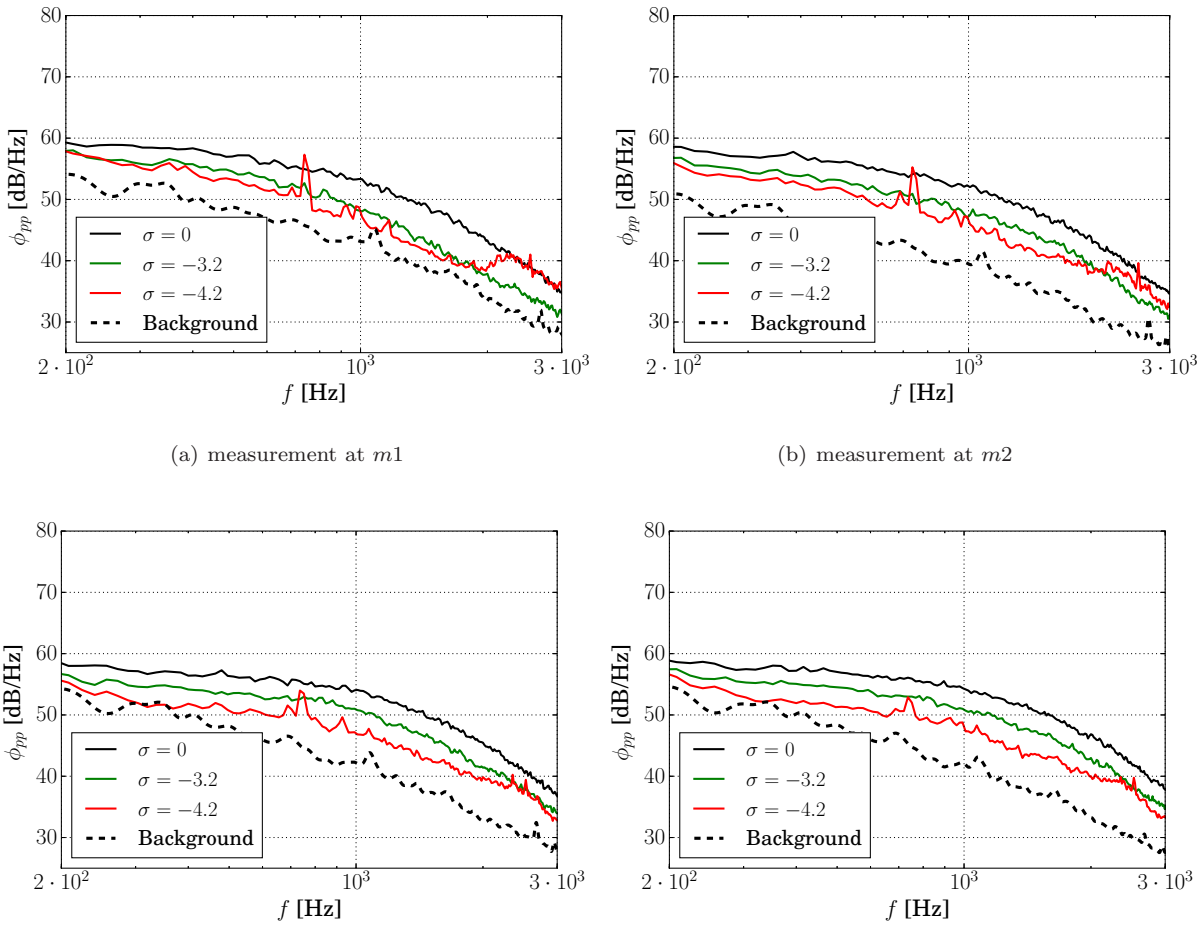

(a) measurement at $m1$

(b) measurement at $m2$

(c) measurement at $m3$

(d) measurement at $m4$

Figure 30. The measured surface pressure fluctuations (ϕ_{pp} [dB/Hz]) in the boundary layer downstream of the active flow control section at locations $m1 - m4$ for the inclined suction flow control cases

The change in the surface pressure fluctuations along the streamwise coordinate downstream of the AFC is presented in Fig. 31. In agreement with the findings on u_{rms}, ϕ_{uu} and ϕ_{pp}, it can be seen that the reduction is almost constant along the streamwise domain. In the inclined suction case, no change in the ϕ_{pp} spectrum was observed, unlike the perpendicular suction where changes in the high and low frequency region were experienced. Similarly to the results presented for the perpendicular suction case, it can be concluded that the inclined suction should be located upstream of the TE to exploit its favourable effects on the TE noise generation driving turbulence quantities. The coherence results for the spanwise microphones near the TE are presented in Fig. 32. Similarly to the perpendicular suction case, the lower suction rate resulted in only a slight increase of γ^2. The higher suction rate of $\sigma = -4.2$ increases the spanwise coherence but the increase is less significant than for the perpendicular suction case. The experienced increase is an indication of the changes in the flow structure, and in particular, the presence of two-dimensional turbulent structures, which becomes more coherent in the spanwise direction with increasing σ.

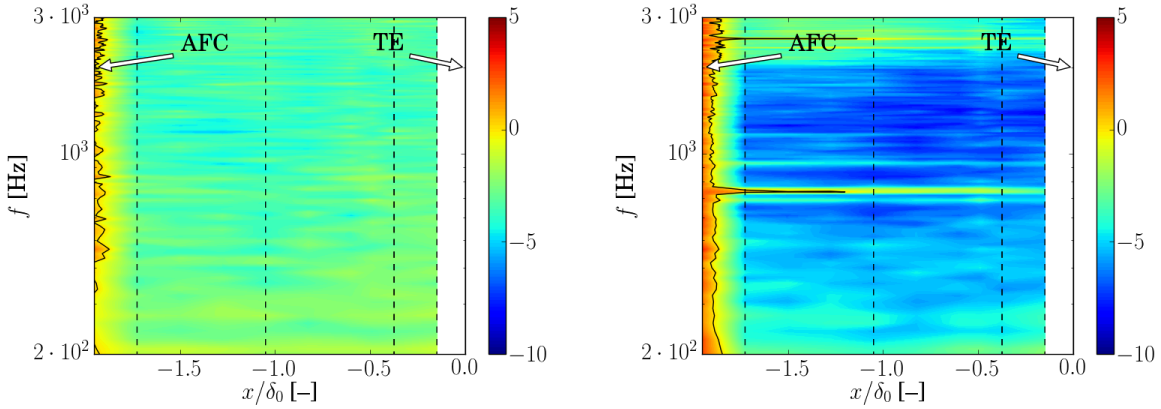

(a) $\sigma = -3.2$ (b) $\sigma = -4.2$

Figure 31. Change in the surface pressure fluctuation spectra ($\Delta\phi_{pp}(x, f)$) downstream of the active flow control section for the inclined suction flow control cases

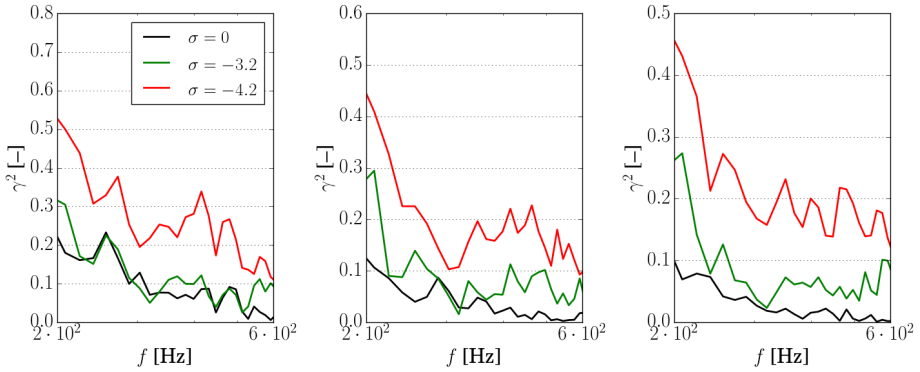

(a) $\Delta x = 3.6$ mm (b) $\Delta x = 7.8$ mm (c) $\Delta x = 11.4$ mm

Figure 32. Spanwise coherence for the inclined suction AFC methods

Table 6. Boundary layer properties at locations $m1$ and $m4$ for the inclined suction cases

	σ [–]	u_∞ [m/s]	δ [mm]	δ^* [mm]	θ [mm]	u_τ [m/s]	Re_θ [–]
$m1$	0	10	25.65	3.87	2.20	0.465	1,500
	−3.2		37.10	3.93	3.21	0.470	2,200
	−4.2		45.88	4.24	3.57	0.470	2,500
$m4$	0	10	27.55	2.79	2.69	0.485	1,800
	−3.2		24.66	1.66	1.41	0.515	1,000
	−4.2		21.34	1.13	0.98	0.520	660

IV. Conclusions

Four active flow control methods including perpendicular and inclined flow suction and injection methods have been investigated for the reduction of trailing edge noise. A comprehensive study is performed using a flat plate with sharp trailing edge to measure the two-dimensional flow field using particle image velocimetry, hot-wire and flush mounted microphones. The paper focuses on the effect of the proposed flow control techniques on the most important trailing edge noise driving components, such as surface pressure fluctuations, boundary layer properties and turbulent length scales, etc.

The investigated blowing control scenarios involved the perpendicular and inclined injection with low flow rates. Both methods resulted in the broadband reduction of the measured surface pressure power spectra. The blowing is effective in shifting the energy containing turbulent structures away from the wall, resulting in a reduction of 10-15 dB in the surface pressure fluctuations. The reduction fades away downstream for the perpendicular blowing case, especially in the low frequency region, due to the induced boundary layer separation. The presence of a shear layer over the separation zone encourages the flow to develop larger energy containing turbulent structures leading to the increase of pressure fluctuations downstream. The inclined blowing is capable of delaying and maintaining the development of energy containing structures, while it is more effective in the reduction of surface pressure fluctuations. It is concluded that the blowing flow control for aeroacoustic tailored purposes should be located close to the trailing edge.

The suction methods can result in a slightly lower reduction of surface pressure fluctuations, but they have a more stable and long lasting effect on the boundary layer. The achieved reduction of 8 dB in the surface pressure fluctuations using flow suction can last even several boundary layer distances downstream of the flow control section. The suction methods were capable of reducing the energy containing eddies resulting in the decrease of the turbulence properties both in the space and frequency domain. The measured pressure spectra showed further decrease at locations downstream of the flow control section, which is believed to be the effect of the break-up of the turbulent structures. The effects of the proposed injection and suction methods on the spanwise coherence of the boundary layer structures and convection velocity near the trailing edge were also studied and it was shown that they can help reshaping the boundary layer in order to reduce the trailing edge noise generation.

Our future work will involve the investigation of turbulent length scales, the resolution of the vorticity transport equation components using particle image velocimetry measurements, additional boundary layer correlation studies and far-field noise measurements. These will help us to better understand the effects of flow control on the trailing edge noise driving turbulence quantities.

References

[1]Williams, J. E. F. and Hawkings, D. L., "Sound Generation by Turbulence and Surfaces in Arbitrary Motion," *Philosopical Transactions of the Royal Society London*, 1969.

[2]Williams, J. E. F. and Hall, L. H., "Aerodynamic sound generation by turbulent flow and in the vicinity of a scattering half plane," *Journal of Fluid Mechanics*, 1970.

[3]Tam, C. K. W., "Discrete tones of isolated airfoils," *The Journal of the Acoustical Society of America*, Vol. 55, No. 6, 1974, pp. 1173–1177.

[4]Amiet, R. K., "Acoustic radiation from an airfoil in a turbulent stream," *Journal of Sound and Vibration*, Vol. 41, No. 4, 1975, pp. 407 – 420.

[5]Amiet, R. K., "Noise Due to Turbulent Flow Past a Trailing Edge," *Journal of Sound and Vibration*, Vol. 47(3), 1976, pp. 387–393.

[6]Chase, D. M., "Noise radiated from an edge in turbulent flow," *AIAA journal*, Vol. 13, No. 8, 1975, pp. 1041–1047.

[7]Brooks, T. F. and Hodgson, T. H., "Trailing Edge Noise Prediction from Measured Surface Pressures," *Journal of Sound and Vibration*, 1981.

[8]Brooks, T. F., Pope, D. S., and Marcolini, M. A., "Airfoil Self-Noise and Prediction," *NASA Report*, 1989.

[9]R. R. Parchen and Technisch Physisce Dienst, "Progress report DRAW: A prediction scheme for trailing edge noise based on detailed boundary layer characteristics," *TNO Report*, Vol. HAG-RPT-980023, 1998.

[10]Lyu, B., Azarpeyvand, M., and Sinayoko, S., "Prediction of noise from serrated trailing edges," *Journal of Fluid Mechanics*, Vol. 793, 2016, pp. 556–588.

[11]Gruber, M., *Airfoil noise reduction by edge treatments*, Ph.D. thesis, University of Southampton, 2012.

[12]Liu, X., Kamliya, H. J., Azarpeyvand, M., and Theunissen, R., "Wake Development of Airfoils with Serrated Trailing Edges," *22nd AIAA/CEAS Aeroacoustics Conference*, AIAA-2016-2817.

[13]Chong, T., Vathylakis, A., Joseph, P., and Gruber, M., "Self-Noise Produced by an Airfoil with Nonflat Plate Trailing-Edge Serrations," *AIAA Journal*, Vol. 51, No. 11, 2013, pp. 2665–2677.

[14]Chong, T. and Joseph, P., "An experimental study of airfoil instability tonal noise with trailing edge serrations," *Journal of Sound and Vibration*, Vol. 332, No. 24, 2013, pp. 6335–6358.

[15]Chong, T., Joseph, P., and Gruber, M., "Airfoil self noise reduction by non-flat plate type trailing edge serrations," *Applied Acoustics*, Vol. 74, No. 4, 2013, pp. 607–613.

[16]Gruber, M., Joseph, P., and Azarpeyvand, M., "An experimental investigation of novel trailing edge geometries on airfoil trailing edge noise reduction," *19th AIAA/CEAS Aeroacoustics Conference*, AIAA-2013-2011.

[17]Azarpeyvand, M., Gruber, M., and Joseph, P., "An analytical investigation of trailing edge noise reduction using novel serrations," *19th AIAA/CEAS Aeroacoustics Conference*, AIAA-2013-2009.

[18]Finez, A., Jondeau, E., Roger, M., and Jacob, M., "Broadband noise reduction with trailing edge brushes," *16th AIAA/CEAS Aeroacoustics Conference*, AIAA-2010-3980.

[19]Herr, M. and Dobrzynski, W., "Experimental Investigations in Low-Noise Trailing-Edge Design," *AIAA Journal*, Vol. 43, No. 6, June 2005.

[20]Geyer, T., Sarradj, E., and Fritzsche, C., "Porous airfoils: noise reduction and boundary layer effects," *15th AIAA/CEAS Aeroacoustics Conference*, No. May, 2009, pp. 1–18.

[21]Geyer, T., Sarradj, E., and Fritzsche, C., "Measurement of the noise generation at the trailing edge of porous airfoils," *Experiments in Fluids*, Vol. 48, No. 2, 2010, pp. 291–308.

[22]Howe, M., "On the Added Mass of a Perforated Shell, with Application to the Generation of Aerodynamic Sound by a Perforated Trailing Edge," *Proceedings of the Royal Society of London. Series A, Mathematical and Physical Sciences*, Vol. 365, No. 1721, 1979, pp. 209–233.

[23]Showkat Ali, S., Liu, X., and Azarpeyvand, M., "Bluff Body Flow and Noise Control Using Porous Media," *22nd AIAA/CEAS Aeroacoustics Conference*, AIAA-2016-2754.

[24]Showkat Ali, S., Szőke, M., and Azarpeyvand, M., "Trailing Edge Bluntness Flow and Noise Control Using Porous Treatments," *22nd AIAA/CEAS Aeroacoustics Conference*, AIAA-2016-2832.

[25]Liu, H., Azarpeyvand, M., Weia, J., and Qua, Z., "Tandem cylinder aerodynamic sound control using porous coating," *Journal of Sound and Vibration*, , No. 334, 2014, pp. 190–201.

[26]Afshari, A., Azarpeyvand, M., Dehghan, A. A., and Szőke, M., "Trailing Edge Noise Reduction Using Novel Surface Treatments," AIAA-2016-2834.

[27]Afshari, A., Azarpeyvand, M., Dehghan, A. A., and Szőke, M., "Three-Dimensional Surface Treatments for Trailing Edge Noise Reduction," *23rd International Congress on Sound & Vibration, Athens, Greece*, 2016.

[28]Clark, I., Baker, D., Alexander, W. N., Devenport, W., Glegg, S. A., Jaworski, J., and Peake, N., "Experimental and Theoretical Analysis of Bio-Inspired Trailing Edge Noise Control Devices," *22nd AIAA/CEAS Aeroacoustics Conference*, 2016, p. 3020.

[29]Clark, I., Alexander, W. N., Devenport, W., Glegg, S. A., Jaworski, J., Daily, C., and Peake, N., "Bio-Inspired Trailing Edge Noise Control," *21nd AIAA/CEAS Aeroacoustics Conference*, 2015, p. 2365.

[30]Ai, Q., Azarpeyvand, M., Lachenal, X., and Weaver, P. M., "Aerodynamic and aeroacoustic performance of airfoils with morphing structures," *Wind Energy*, Vol. 19, No. 7, 2016, pp. 1325–1339, we.1900.

[31]Hartwich, P. M., Dickey, E. D., Sclafani, A. J., Camacho, P., Gonzales, A. B., Lawson, E. L., Mairs, R. Y., and Shmilovich, A., "AFC-Enabled Simplified High-Lift System Integration Study," 2014.

[32]Koklu, M., "Effect of a Coanda Extension on the Performance of a Sweeping Jet Actuator," *AIAA Journal*, Vol. 54, 2016, pp. 1125–1128.

[33]Antonia, R. A. ., Fulachier, L., Krishnamorthy, L. V., Benabid, T., and Anselmet, F., "Influence of wall suction on the organized motion in a turbulent boundary layer," *Journal of Fluid Mechanics*, Vol. 190, 1988, pp. 217–240.

[34]Antonia, R. A., Zhu, Y., and Sokolov, M., "Effect of concentrated wall suction on a turbulent boundary layer," *Physics of Fluids*, Vol. 7, No. 10, 1995, pp. 2465–2474.

[35]Park, J. and Choi, H., "Effects of uniform blowing or suction from a spanwise slot on a turbulent boundary layer flow," *Physics of Fluids*, Vol. 11, 1999, pp. 3095.

[36]Oyewola, O., Djenidi, L., and Antonia, R., "Combined influence of the Reynolds number and localised wall suction on a turbulent boundary layer," *Experiments in Fluids*, Vol. 35, No. 2, 2003, pp. 199–206.

[37]Oyewola, O., Djenidi, L., and Antonia, R., "Influence of localised wall suction on the anisotropy of the Reynolds stress tensor in a turbulent boundary layer," *Experiments in Fluids*, Vol. 37, No. 2, 2004, pp. 187–193.

[38]Oyewola, O., Djenidi, L., and Antonia, R., "Influence of localised double suction on a turbulent boundary layer," *Journal of Fluids and Structures*, Vol. 23, No. 5, 2007, pp. 787 – 798.

[39]Wolf, A., Lutz, T., Würz, W., Krämer, E., Stalnov, O., and Seifert, A., "Trailing edge noise reduction of wind turbine blades by actice flow control," *Wind Energy*, Vol. 1737, 2014.

[40]Lutz, T., Arnold, B., Wolf, A., and Krämer, E., "Numerical Studies on a Rotor with Distributed Suction for Noise Reduction," *Journal of Physics: Conference Series*, Vol. 524, No. 1, 2014, pp. 012122.

[41]Matera, D., *Validation of the noise prediction code Rnoise and reduction of trailing edge noise by active flow control*, Ph.D. thesis, Universita Degli Studi Di Padova, 2013.

[42]S. R. Koh and W. Schroder and M. Meinke, "Sound Generation Control by Fluid Bleeding," *15th AIAA/CEAS Aeroacoustics Conference*, May AIAA-2009-3225.

[43]Koh, S. R., Schröder, W., and Meinke, M., "Numerical Study of Noise Reduction via Wall Turbulence Control," *16th AIAA/CEAS Aeroacoustics Conference*, AIAA-2010-3990.

[44]Brookfield, J. M. and Waitz, A., "Trailing-Edge Blowing for Reduction of Turbomachinery Fan Noise," *Journal of Propulsion and Power*, Vol. 16, No. 1, Jan-Feb 2000.

[45]Kline, S. J. and McClintock, F. A., "Describing uncertainties in single-sample experiments," *Mechanical Engineering*, Vol. 75, No. 1, Jan 1953, pp. 3–8.

[46]Schewe, G., "On the structure and resolution of wall-pressure fluctuations associated with turbulent boundary-layer flow," *Journal of Fluid Mechanics*, Vol. 134, 9 1983, pp. 311–328.

[47]Corcos, G. M., "Resolution of Pressure in Turbulence," *The Journal of the Acoustical Society of America*, Vol. 35, No. 2, 1963, pp. 192–199.

[48]Barrett, R. V., "Design and performance of a new low turbulence wind tunnel at Bristol University," *Aeronautical Journal*, 1984.